Fibrous Scaffolds for Building Hearts and Heart Parts

A. K. Capulli[1], **L. A. MacQueen**[1], **Sean P. Sheehy**, and **K. K. Parker**[*]

[*]

Abstract

Extracellular matrix (ECM) structure and biochemistry provide cell-instructive cues that promote and regulate tissue growth, function, and repair. From a structural perspective, the ECM is a scaffold that guides the self-assembly of cells into distinct functional tissues. The ECM promotes the interaction between individual cells and between different cell types, and increases the strength and resilience of the tissue in mechanically dynamic environments. From a biochemical perspective, factors regulating cell-ECM adhesion have been described and diverse aspects of cell-ECM interactions in health and disease continue to be clarified. Natural ECMs therefore provide excellent design rules for tissue engineering scaffolds. The design of regenerative three-dimensional (3D) engineered scaffolds is informed by the target ECM structure, chemistry, and mechanics, to encourage cell infiltration and tissue genesis. This can be achieved using nanofibrous scaffolds composed of polymers that simultaneously recapitulate 3D ECM architecture, high-fidelity nanoscale topography, and bio-activity. Their high porosity, structural anisotropy, and bio-activity present unique advantages for engineering 3D anisotropic tissues. Here, we use the heart as a case study and examine the potential of ECM-inspired nanofibrous scaffolds for cardiac tissue engineering. We asked: *Do we know enough to build a heart?* To answer this question, we tabulated structural and functional properties of myocardial and valvular tissues for use as design criteria, reviewed nanofiber manufacturing platforms and assessed their capabilities to produce scaffolds that meet our design criteria. Our knowledge of the anatomy and physiology of the heart, as well as our ability to create synthetic ECM scaffolds have advanced to the point that valve replacement with nanofibrous scaffolds may be achieved in the short term, while myocardial repair requires further study in vitro and in vivo.

Graphical Abstract

Corresponding author: Kevin Kit Parker, Ph.D., Disease Biophysics Group, Wyss Institute for Biologically Inspired Engineering, John A. Paulson School of Engineering and Applied Sciences, Harvard University, 29 Oxford St, Pierce Hall 321, Cambridge MA 02138, kkparker@seas.harvard.edu.
[1]These authors contributed equally to this work.
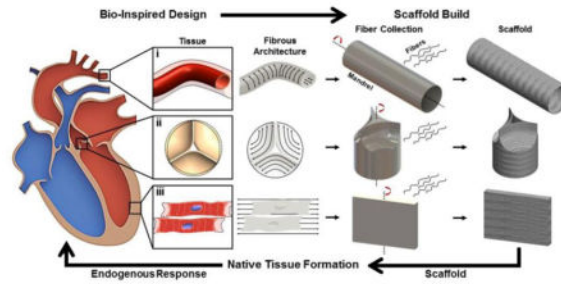
Keywords

Nanofiber; scaffold; electrospinning; force spinning; rotary jet spinning; cardiac; myocardium; valve; tissue engineering; regenerative medicine

1. Introduction

In their 2002 *Viewpoint* article, Hench and Polak [1] described a transition to —Third-Generation Biomedical Materials that stimulate specific cellular responses to promote endogenous tissue regeneration and help the body to heal itself. To accomplish this goal, implanted scaffolds should first minimize toxic response in the host and subsequently recapitulate properties of the native tissue's extracellular matrix (ECM) to promote cell assembly into functional tissues. Mechanotransduction through the cell-ECM interface plays a fundamental role in regulating tissue homeostasis, growth, and regeneration [2–7]. In muscular organs, ECM morphology and elasticity regulate cell shape and coordinate myofibril assembly, thereby influencing tissue architecture and contractile strength [8–11]. Specifically in the heart, a fibrillar ECM network provides guidance cues that direct the spatial and temporal synchrony of cardiac development. Thus, recapitulation of this ECM network using fibrous materials may be a crucial design consideration of engineered cardiac tissues. We therefore asked whether fiber-based scaffolds can be used to guide the assembly of functional cardiac tissues.

The use of fibrous cell culture substrates to study tissue regeneration can be traced back at least a century to the work of Ross Granville Harrison who, in 1914 [12], cultured embryonic frog and chick cells on spider silk, noting that —the solid support influence[d] the form and arrangement assumed by the moving cells and cells were —arranged with reference to the web fibers, and they [were] usually drawn out into long processes . Contact guided cell growth was subsequently studied on diverse substrates (e.g., glass fibers [13], oriented collagen [14] and micropatterned features [15]) but predictable tissue assembly required discovery and classification of tissue-specific structures, cell types, cell adhesion proteins [16–19], and their interactions with the extra-cellular microenvironment [4, 20, 21]. Extensive study of these components and properties of cell-ECM interaction provide a mechanistic understanding of tissue self-assembly that can be incorporated into the design specifications of engineered tissues to guide the development of more physiologically-relevant cellular scaffolds [22–24]. Scaffolds composed of fibrous materials are increasingly used for regenerative medicine because fiber manufacturing platforms now exist capable of producing fibers with a wide range of structural and biochemical properties [25–29]. Fiber

scaffolds fabricated using these techniques can mimic the native ECM and be woven or otherwise assembled into organ-scale structures with adequate porosity and structural stability to support cell infiltration and assembly [30]. Moreover, the incorporation of bioactive molecules into synthetic fibrous scaffolds, such as native ECM components and growth factors, may enhance the development of engineered tissues into more accurate tissue analogs and promote healthy integration into diseased or injured tissues [31].

In this review, we focus on the use of fibrous scaffolds for cardiac tissue repair because the heart is one of the least regenerative organs in the body [32] and natural healing processes can result in deleterious remodeling following insult or disease [33, 34]. We narrow our focus to the myocardium and aortic valve to illustrate the diversity of the heart's sub-structures and the unique requirements for distinct repair strategies. We begin by summarizing properties of the myocardium and heart valves that serve as design criteria for scaffolds. These include multiscale structural and functional properties of the ECM, cells, tissues, and organs that we tabulate and rank according to their current utility in engineering design. We then describe scaffold manufacturing platforms and assess their capabilities to produce scaffolds that meet our design criteria. The effectiveness of nanofibrous scaffolds to promote cardiac cell assembly into functional myocardial tissues is examined by highlighting in vitro and in vivo use of bioactive myocardial patches. Exploratory experiments using myocardial patches provide a test bed for biotic-abiotic interface optimization aimed at restoring tissue-level function. This is important because although heart function can be restored by abiotic prosthetics [35], regenerative strategies that address biological aspects of heart function may improve host integration for more permanent and adaptive repair while eliminating the need for external power sources that currently hamper abiotic artificial hearts and increase the patient's risk of infection. Crucially, cardiac tissue engineering provides increasingly accurate in vitro models of cardiac health and disease for drug discovery [36, 37], cardiac stem cell biology [38–41], and cell-ECM interactions [33, 42, 43].

2. Design Criteria for Engineered Cardiac Tissues

The heart is a muscular pump tasked with continuously providing efficient blood transport throughout the body. This is achieved through hierarchical control of structure and function integrated over multiple spatial scales [2, 6]. A key challenge in the field of tissue engineering is defining the standards by which successful replication of native tissue function is achieved, particularly in light of increasing demand for patient-relevant tissue models created using human stem cells. What metrics should be used to determine the success of an engineered tissue fabricated using a fibrous scaffold? Physical material properties, two dimensional planar alignment and three dimensional architecture are important aspects of native tissues that must be recreated in engineered scaffolds to guide cellular self-assembly. Additionally, biochemical properties, degradation kinetics, and bioactive components must be optimized to recapitulate or trigger specific in vivo responses and tissue development in engineered tissues meant for implantation.

In order to fabricate biomimetic tissues that recapitulate the function of the heart, it is first necessary to quantitatively define the relevant structural and performance attributes that

define normal physiological function. Although the standard comparison for the developed functionality of an engineered tissue is the native tissue it is designed to repair or replace, should native tissue chemical and mechanical properties also serve as design criteria for fiber scaffolds? Alternatively, should some immature or basic model of the tissue structure and composition be the standard for a fibrous scaffold: a structure and composition that will best initiate scaffold remodeling and tissue formation once implanted? Measurements of physical features and functional outputs, such as those listed in Table 1, can be used to define target values that serve as quality control metrics for assessing the degree to which engineered tissues faithfully mimic their native counterpart (Fig. 1A). Comprehensive, quantitative comparison of engineered tissues versus healthy, mature tissues using machine learning approaches [44, 45] and statistical metrics, such as strictly standardized mean difference, could provide robust, standardized quality assurance rubrics for determining the fitness of engineered tissues for regenerative therapy applications [46]. Traditional tissue engineering approaches involve scaffold to tissue fabrication: scaffold production, in vitro cell seeding, in vitro cell-scaffold conditioning to form tissue, and finally implantation. At each phase, metrics are defined to determine success. For example, mechanical/chemical properties of the raw scaffold, efficiency of seeding, degree of remodeling by the cells during conditioning in vitro, and the eventual functionality of the implanted construct. Most importantly, these metrics help to answer the question: *Can we build a heart?* by allowing one to determine which aspects of tissue structure and function are well defined, and which require further investigation (Fig. 1B). Below, we describe key structural and functional properties of the myocardium and cardiac valves that serve as design criteria for engineered fibrous scaffolds capable of restoring normal function after injury or disease.

2.1 Multiscale structure of striated heart muscle

Anisotropic tissue architecture is a hallmark of heart muscle which may be recapitulated using nanofibrous scaffolds. It has been shown that the heart can be unraveled (Fig. 2A) [47] to reveal a helical-laminar assembly of hierarchically organized fibrillar structures: Epiphyseal fibers surround the myocardium, perimysial fibers surround groups of cardiomyocytes, and endomysial fibers wrap individual cardiomyocytes [48]. Individual myofibers contain chains of contractile cardiomyocytes that are physically connected by intercalated discs that contain gap junctions which provide electrical continuity and are surrounded by the perimysial ECM (Fig. 2B). Perimysial fibers are mostly parallel with the long axis of the muscle and contribute to the directional contraction of cell bundles [49]. Helically overlapping myocardial fibers are arranged into distinct laminas four to six myocytes thick and separated from adjacent laminas by an extracellular collagen network [50].

The complete arrangement of bundled myofibers around the ventricles forms a helicoid that economizes fiber length and optimizes ejection fraction during ventricular contraction (Fig. 2C) [51]. The complex geometry of the heart arises from precisely choreographed cellular interactions with soluble factors, neighboring cells, and the ECM that guide cellular fate decisions at each stage of development [52–54]. Boundary conditions presented by the ECM potentiate precise and predictable parallel alignment and bundling of myofibrils as they organize within and across cell boundaries during cardiomyocyte development [55–57].

Physical interactions between cardiomyocytes and the ECM mediate transmission of a variety of signaling cues that act through a mechanical linkage with the cardiomyocyte cytoskeleton (CSK) that may influence the activation of gene expression programs that direct changes in phenotypic state [2, 11, 58–62]. In the heart, physical attachment of the cardiomyocyte CSK to the surrounding ECM is mediated by costameres, vinculin-containing rib-like bands localized to the z-discs of sarcomeres (Fig. 2D), that encircle the cardiomyocyte perpendicular to its long axis. They serve as sites for cell attachment, bidirectional mechanotransduction between the cell and ECM [63], and mechanical load-dependent modulation of cardiomyocyte development and pathophysiology [64–66]. Regionalized differences in structural and mechanical cues imparted on cardiomyocytes over the course of heart development activate gene regulatory networks that drive cells toward the cell fate attractor states necessary for chamber specification [11, 52, 62, 67]. Alterations in the mechanical load on the heart during physiological and pathological hypertrophy have been shown to activate distinct gene expression programs to provide context-specific cellular responses aimed at maintaining heart function in response to the dynamic physical microenvironmental cues elicited in these conditions [68]. In the healthy myocyte, integrins are commonly localized within costameres, anchoring the sarcomeric z-discs in the outer most regions of the myofibrillar array [2]. In long-term monolayer culture, cardiomyocytes remodel their adhesive structures and reorganize costameres into planar focal adhesions found in nonmuscle cells [69] suggesting that cardiomyocyte contractility would be optimal in a 3D ECM environment that allows the adoption of the rod-like architecture that typifies the adult myocardium. Further, the native myocardial ECM supports dynamic mechanical loading that places specific requirements on surrogate materials used in myocardial tissue engineering to provide an appropriate set of physical cues that activate the gene regulatory networks that give rise to desirable structural and functional properties.

The relative proportions of ECM proteins such as collagens, fibronectin, and laminin, change during development and maturation of myocardial tissues, reflecting developmental stage-dependent differences in regenerative capacities arising from this shift in ECM composition (Table 2). It has been shown that cardiomyocytes are sensitive to the increase in microenvironmental elasticity that results from increased collagen I expression during development, demonstrating an increase in myofibril protein expression and sarcomere alignment with increased tissue elasticity [70]. The adult myocardium is one of the least regenerative tissues in the body and cardiomyocyte deficiency underlies most causes of heart failure [32]. Cardiomyocyte renewal rates in the postnatal heart are not definitively known [71]: Bergmann et al. [72] estimated that ~50% of cardiomyocytes are renewed over a normal human lifespan but higher rates were reported in young adults by Mollova et al. [73]. There is also evidence that in both neonatal and adult mammals, proliferation of pre-existing cardiomyocytes contributes to myocyte turnover [74] and that myocyte turnover can be enhanced by the ECM [43]. Further elucidation of the role that the ECM plays in regulating myocyte proliferation may provide a possible strategy to engineer scaffolds that recapitulate the endogenous myocardial regenerative capacity observed during early stages of heart development. This forms the basis of a vertically-integrated developmental build

that gives rise to synchronous formation of the heart chambers and the supporting components that allow coordinated electrical and contractile function.

2.2 Cardiac pacing

Cardiac contractions are controlled by the sinoatrial (SA) node and Purkinje fibers that form a specialized excitatory and conduction system [75]. The SA node is the pacemaker of the heart, responsible for initiation of the heartbeat and the branching Purkinje fibers ensure that impulses are rapidly conducted throughout the heart to synchronize contraction and optimize ejection fraction. Life-threatening arrhythmias resulting from dysfunctional pacing have been revolutionized by electronic pacemakers but their reliance on batteries and electronic control systems highlight potential advantages of biological or bio-electronic tandem approaches to cardiac pacing [76, 77], including genetic engineering [78] and cell implantation [79]. The recent advent of cardiac optogenetics, where transgenic expression of light-gated ion channels permits optical control of cardiac pacing [80, 81] and termination of reentrant electrical activation [82] (e.g., spiral waves), suggests that gene and cell delivery methods can be used to impart light sensitivity on cardiac tissues for - low-energy pacing of target cells [83]. In addition to the promise of optogenetics for developing improved tissue engineered pacemakers, it is also necessary to faithfully recapitulate the anisotropic electromechanical syncytium of healthy myocardial tissue to ensure proper electrical propagation and contractile synchrony.

2.3 Multiscale functional properties of striated heart muscle: conduction and contraction

In order to maintain efficient heart function, the myocytes comprising the myocardium must maintain parallel alignment of sarcomeres and form electro-mechanical linkages between individual cardiomyocytes comprising myocardial tissues to ensure coordinated activity across multiple spatial scales, up to the organ level (Fig. 3A). At the nanoscale, CSK/ECM coupling ensures that cardiomyocyte CSK and motor units align in the direction of the ECM for coordinated propagation of excitation wavefronts through gap junctions in the cardiac musculature. Interruption of the ordered wavefront propagation can be arrhythmogenic and is associated with various cardiomyopathies [2]. Conduction velocity (CV) is consistently greatest in the fiber direction such that longitudinal CV_L exceeds transverse CVT by a factor of ~2–10, depending on measurement region and pacing rate (Table 3) [84, 85]. 3D mapping of activation projected onto tissue structure reveals that electrical activity spreads in three distinct directions from an intramural LV point stimulus, corresponding with local microstructural axes [86]. Active electric properties were determined to be anisotropic transverse to the myofiber direction, and principal local CVs in the fiber direction and transverse to it were 67 ± 1.9, 30 ± 1, and 17 ± 0.4 cm/sec (anisotropy ratios: 4:1 & 8:1). The laminar architecture of ventricular myocardium thus gives rise to orthotropic electric properties with slow propagation normal to laminae [86, 87].

Contractile force generated by the heart increases with increasing myocardial strain during diastole. This fundamental property whereby the heart synchronizes cardiac output with venous return is known as the —Frank-Starling Law and was appreciated by 19th century physiologists [88]. We now know that calcium-dependent activation of sarcomeric proteins underlies this length-tension relationship [89–95] and tension generated by individual

cardiomyocytes depends on cell and sarcomere length, SL (Fig 3B, C, Table 4) [96–99]. As summarized by Shiels & White [96] in their commentary on the Frank–Starling mechanism in vertebrate cardiomyocytes, end systolic SL ~1.9–2.0·µm and end diastolic SL ~2.2–2.4·µm. SL-dependent cardiomyocyte contractile force scales to volume-dependent ventricle contractile force and stroke work due to coordinated activity of the myocardial syncytium.

Conduction velocities are generally lower in engineered tissues than in whole organs. Whereas longitudinal and transverse conduction velocities (CV_L and CV_T, respectively) are on the order of CV_L ~ 20 cm/s and CV_T ~ 10 cm/s for engineered tissues, they are CV_L ~70 cm/s and CV_T ~25 cm/s for whole human left ventricles (Table 3). Conduction velocity depends on gap junctional conductance (in silico: [100]) that is partly determined by the activity of gap junction channel proteins, the assembly and function of which may be limited in vitro using previously dissociated cells [101]. Similarly, contractile stresses generated by whole organs are larger than those generated by engineered tissues. Whereas human LV contractile stresses are on the order of 100 kPa, human ventricular muscle strips generated ~40 kPa and hESC-CM ~12 kPa (Table 4). This discrepancy is expected when immature stem cell-derived cardiomyocytes are used to build tissues or when cells that are isolated from patients loose function in vitro. As with the case of conduction velocities, this discrepancy may arise, at least in part, from non-ideal cell connectivity. We expect improved stem cell maturation protocols and in vitro culture methods to reduce the gap between engineered and natural tissue contractile stress generation capacity. Fibrous scaffolds can play a significant role here, as they provide 3D in vitro cell culture substrates that can guide cardiomyocyte assembly and promote functional maturation.

2.4 Ventricle Elastance and Strain

Myocardial tissue is mechanically dynamic with time-dependent elastic properties, some of which are listed in Table 5. Ventricular end systolic/diastolic pressure/volume relations (ESPVR/EDPVR) are used to estimate LV elastance in systole or diastole [102]. Shear stiffness during LV contraction closely matches chamber pressure during diastole, and systole (Fig. 3D), demonstrating the importance of designing fibrous scaffolds capable of withstanding dynamic changes in the mechanical environment [103]. In contrast to the nonlinear EDPVR, the ESPVR is approximately linear over a wide range of conditions and its slope, E_{es}, known as end systolic elastance, can be accurately measured non-invasively [104]. Ees and the slope of EDPVR at low volumes represent the maximum and minimum, respectively, of the time-dependent elastance, E(t) (Fig. 3E). Typical values for E_{es} summarized by Gayat et al.[105] are: Ees ~2.0 mm Hg/ml in normal hearts, E_{es} <1.0 mm Hg/ml in dilated failing hearts and E_{es} ~4.0 mm Hg/ml inhypertrophied hearts.

Myocardial tissue is subjected to significant mechanical strain, often exceeding 20% between systole and diastole, depending on the location within the left ventricle (Table 6). Increased myocardial stiffness is associated with elevated end diastolic pressure in pressure-overloaded but not volume-overloaded ventricles [106]. Zhang et al. [107] found longitudinal and circumferential strain, as well as strain rate, to be highly correlated with E_{es}. This suggests that, because these measures reflect chamber elastance and contractility,

strain measurements provide added value to ejection fraction in the prediction of adverse outcomes.

2.5 Cardiac Valve Structure

Cardiac valves maintain unidirectional blood flow through the heart by coordinated action of thin membranous structures known as leaflets or cusps. Key structural and functional properties of the cardiac valves are summarized in Table 7. Valve tissue undergoes significant remodeling throughout life and in response to environmental stimuli [139]. However, aberrant valve remodeling can lead to valvular diseases that alter blood flow and mechanical loads placed on the myocardium, ultimately disrupting broad aspects of cardiac function [140, 141]. During the cardiac cycle, increased or decreased left ventricular pressure in systole or diastole, respectively, force the aortic valve leaflets to open and close (Fig. 4A), a process that is repeated ~3 billion times over the course of an average lifetime [142]. Aortic valve leaflets contain three layers with collagen fibers predominant in the fibrosa, a GAG-rich matrix in the spongiosa, and elastin sheets in the ventricularis [143]. Collagen fibers within the valve leaflets are load bearing during diastole (closure) and oriented principally in the circumferential direction. Elastin fibers are responsible for leaflet recoil during systole (opening) and are principally oriented in the radial direction of the leaflet (Fig. 4B). Disoriented ECM fibers are a hallmark of valve disease (Fig. 4A) although their exact orientation and bundle size is distinctive to each leaflet (Fig. 4C). To study the effects of collagen fiber alignment on valve kinematics and hemodynamics, Marom et al. [144] used numerical fluid-structure interaction models of asymmetric mapped collagen fiber networks from measurements of porcine valve and a simplified-symmetric network (Fig. 4C). They showed that fibers carried most of the mechanical load and asymmetric internal structure had a considerable impact on the hemodynamics. Regions with less dense fiber network were subjected to higher internal stress and flow shear stress magnitudes and, therefore, are at higher risk of damage. Numerous attempts have been made to fabricate tissue engineered scaffolds that recapitulate the structure and function of native heart valves [169, 217–219]. By constructing the trileaflet global structure of semilunar valves using fibrous material, in vitro cell seeding allows for physiologically-relevant conditioning that provides structural and mechanical cues for tissue formation before implantation.

Cardiac valves exhibit pronounced structure-function relationships that are often disrupted in valvular heart disease (VHD) and result in abnormal valve leaflet number, morphology, mechanical properties, and/or biochemical composition [145–147]. For example, calcific aortic valve disease initiation is associated with fibrotic collagen accumulation and disorientation, which leads to thickened, stiffened valve leaflets and a deterioration in function [148]. Valve leaflets contain valvular interstitial cells (VIC) and the leaflets are coated by a monolayer of valvular endothelial cells (VEC) that are in contact with circulating blood. VICs are associated with remodeling and repair [149] but their dysregulation can lead to leaflet fibrosis and calcification that progress to sclerosis and stenosis [140, 150]. VECs suppress VIC pathological differentiation into α-SMA positive myofibroblasts, an effect that is enhanced by exposure of the endothelium to flow-induced shear stress [151]. VECs also undergo endothelial-mesenchymal transformations during valve development and may replenish VIC populations [152]. For these reasons, there is

hope that endothelial cell recruitment to valve scaffolds can lead to functional VEC leaflet coating and EMT-based repopulation of interstitium. Because circulating endothelial progenitors are rare [153], a strategy based on endothelial recruitment from vascular structures adjacent to the implanted scaffold seems favorable. Fibrous scaffolds may provide structural cues required to initiate endothelial cell recruitment either from circulating blood or from the border zone adjacent to implanted scaffolds. Fibrous scaffolds may provide structural cues required to initiate endothelial cell recruitment and serve as a substrate to recapitulate the valve interstitium for VIC regulation.

3. Fibrous Scaffold Production Techniques

Nanofibers with high surface area to volume ratios and small diameters mimic ECM structure, thus providing suitable substrates for regenerative tissue growth. Three prominent nanofiber scaffold production methods are illustrated in Fig. 5 including decellularization of tissues (Fig. 5A), electrospinning (Fig. 5B), and Force Spinning (Fig. 5C). The respective advantages and disadvantages of these methods are outlined in Table 8, and properties of fibrous scaffolds produced by these methods are listed in Table 9. Structural properties such as fiber diameter size, thickness, and porosity are tuned in these scaffolds to allow cellular integration and tissue formation. The biomechanical composition of scaffolds is tailored to recapitulate the native tissue chemistry and mechanics as instructive cues for specific tissue formation. For example, heart valve tissue scaffold porosity must be tuned to allow cell infiltration but limit vascularization while an elastic material (i.e. elastin) oriented radially will provide scaffold recoil and a strong material (i.e. collagen) oriented circumferentially will provide structural integrity. Although decellularized tissues and organs provide 3D substrates for tissue regeneration, the lack of experimental control over constituent components hinders reproducibility of scaffold composition and reduces predictability of cell response to the scaffold. Emerging fiber production techniques aim to overcome these limitations using a —bottom-up approach to scaffold engineering where each scaffold component (e.g., ECM bioproteins) and structure is precisely controlled.

3.1 Decellularized Extracellular Matrix Fibrous Scaffolds

The decellularization of allogeneic or xenogeneic tissues may be the most structurally and compositionally relevant method to fabricate fibrous scaffolds for regenerative tissue engineering (Fig. 5A). A fully decellularized tissue, in theory, will retain the fibrous, three dimensional structure and organization of its constituent protein ECM providing the exact scaffolding framework of a specific organ [166]. Decellularizing tissues is rooted in the successes of transplanted cadaveric and donor tissues; by further removing the native cells of a transplant tissue, the aim is to avoid the risk of rejection and be able to —customize the tissue with a different native or stem cell based population of cells [164]. Physical, chemical and enzymatic treatments are used to decellularize tissues [167, 168], including lungs [169], kidneys [170], heart [171], bone [172], and vasculature [173]. Recently, a detergent based treatment protocol using both antegrade and retrograde perfusion through the native tissue vasculature at low relative physiological pressures was published for the effective decellularization of whole hearts, lungs, and kidneys [174]. The maintained vasculature of decellularized tissues provides not only the necessary access to the tissue for

decellularization, but also serves as a recellularization conduit and nutrient transport system in the regenerating tissue. Reseeded, whole heart scaffolds produced by perfusion methods have even been shown to develop immature organ-level function in vitro such as electrical conduction and mechanical function (pumping/contraction) of the reseeded heart [175, 176]. The return of some organ level function demonstrates that decellularized tissues may provide a viable source of fibrous scaffold with the architectural and compositional cues necessary to potentiate tissue regeneration.

Although decellularized tissues and organs can provide fibrous scaffolds that resemble native structure and biochemical composition, matching these properties to specific patient needs is challenging. The matrix necessary and sufficient to activate immature resident stem cell populations and regulate the development of these cells into mature tissues remains unclear and is not controlled experimentally when using developmentally mature decellularized tissues. Furthermore, there exist many unique processing methods that attempt to sufficiently decellularize the tissue while minimizing ECM deterioration and aberrant host inflammatory responses [177, 178]. This diversity in the field has resulted in a lack of minimum standards for determining successful decellularization and host reactions to organ- or tissue-based fibrous scaffolds [167].

3.2 Synthetically Produced Fibrous Scaffolds

Synthetic fibrous scaffold production and evaluation can be subject to higher degrees of manufacturing control than tissue decellularization. This lends itself to the introduction of good manufacturing procedures and increased reproducibility and reliability. The most popular method of fabricating nanofiber scaffolds via synthetic engineering is electrospinning (Fig. 5B). Electrospinning is the process by which an electrically charged polymer melt or solution is extruded through an orifice, creating a jet that solidifies into nanofibers that are subsequently collected on a substrate [179]. Numerous methods now exist to electrospin nanofibers, including traditional needle arrays and needle-free techniques [25, 26] developed to improve fiber formation and production rates: these include bubble electrospinning [180] and microfluidic electrospinning [181]. Synthetic polymers and biological proteins are electrospun using these techniques independently [182, 183] or in combination [184, 185]. The diversity of electrospinning techniques and electrospun materials has translated to numerous fibrous tissue engineering applications including ligament, tendon, skeletal muscle, skin, blood vessel, and neural scaffolding [186].

The diversity of electrospinning techniques and applications result from controlled engineering design and fabrication processes. Unlike decellularized tissue scaffolds manufactured using top-down approaches, synthetic electrospun scaffolds are built — bottom-up. Because of this —bottom-up approach, scaffold characteristics such as fiber diameter [187], fiber alignment [26], scaffold porosity for cell infiltration [188], and macroscopic scaffold geometry [189] can be controlled by simply varying needle diameter, applied needle voltage, flow rate or viscosity of solution/melt, along with a number of other spinning parameters [190]. In addition to control over these physical characteristics, electrospun scaffolds can be bioactively functionalized with the inclusion of drugs [191] or specific growth factors [192] within the fibers to guide host response and endogenous repair

mechanisms. Recently, electrically conductive fibers [193] and metabolic sensors [194, 195] have been incorporated into smart' electrospun scaffolds for real-time tissue performance monitoring. Since electrospun fibers are built by a —bottom-up, fiber-by-fiber approach, they can be biomechanically tuned and functionalized for specific tissue scaffolding.

However, it is also this fiber-by-fiber approach to creating scaffolds with electrospinning that limits its utility as a manufacturing method. Production rates of electrospun fibers are very low compared to industrial fiber production techniques; the most productive industrial scale electrospinning systems hardly reach kilograms of fibers per hour whereas common industrial scale melt or wet spin fiber production can reach tens of tons of fibers per hour [196]. Although numerous multi-needle setups have been developed to increase fiber production rates [197], these methods complicate the normally simple electrospinning setup which makes it an attractive manufacturing technique by introducing multiple electric fields and numerous high voltage connections. Additionally, because of this high voltage required to electrospin, material and solvent choice for electrospinning is limited to polymers that are soluble in conductive solvents. This is particularly restrictive for electrospinning regenerative scaffolds made of or including protein due to the detrimental effects of voltage and solvent on protein three dimensional structure [198]. Melt-electrospinning processes have been developed to address the limitations of solvents [199], though the resultant fibers generated are commonly on the order of microns in diameter and the high temperature of the melt process likely has a denaturing effect on electrospun proteins and stability of synthetic polymers. Production rate and material manufacturing limitations have limited the translation of electrospun fibrous scaffolds to industrial-scale production.

In order to overcome the manufacturing limitations of electrospinning, force-based fiber fabrication via Rotary Jet Spinning (RJS) [28] was developed for the fabrication of fibrous scaffolds (Fig. 5C). RJS uses the centrifugal forces developed in a rotating reservoir perforated with a single or multiple micron-scale orifices to circumferentially extrude nanofibers from solution. By varying polymer solution and spinning parameters (e.g. solution viscosity, rotation rate and extrusion speed), nanofiber properties such as fiber diameter and alignment can easily be controlled using the RJS fabrication technique [200]. Production rates achievable by a single force driven system (~100 g/hr) are roughly two orders of magnitude higher than similarly scaled electrospinning systems. Collagen and gelatin nanofibers are rapidly fabricated with the RJS both with and without mixing with synthetic polymers to tune mechanical properties and degradation profiles of scaffolds [29]. In addition to collagen and gelatin, the high shear forces developed in the orifice of the RJS reservoir during extrusion has been exploited to initiate fibrillogenesis of beta sheet rich proteins such as silk to produce insoluble, pure protein nanofibers without the need of post-processing crosslinking [201]. Overcoming the production rate limitations of electrospinning while maintaining, and even increasing, the versatility of spinning materials, RJS and similar force spinning techniques [202] bring synthetic nanofiber based scaffold fabrication processes closer to true manufacturing and clinical translation.

The challenge of any synthetic fiber fabrication technology is building the global, three dimensional structure of the target cardiac tissue; that is, the three dimensional collection of fibers. Because of the —bottom-up approach of synthetic fibrous scaffold fabrication,

building from the nano and micron scales of single fibers to the macro-scale geometries of scaffold tissues requires innovative, cumulative fiber collection techniques. Using electrically grounded plates, cylindrical mandrels, and other specially shaped columnar collectors for example, various geometries can be manufactured via electrospinning fibers to achieve specific tubular fibrous structures. These innovative fiber collection strategies suggest that full multiscale recapitulation of tissue and organ structures will soon be possible using nanofiber production platforms such as electrospinning and force spinning.

4. Cardiac Tissue Repair Using Fibrous Scaffolds

The overall strategy for designing synthetic cardiac tissues using bio-inspired nanofibrous scaffolds is summarized in Fig. 6. Given the complexity involved in assessing the quality of traditional tissue engineered products that are seeded, cultured, and conditioned in vitro, how practical—logistically—is their translation to common usage in the clinic? There are currently no standardized guidelines for determining the fitness of engineered heart tissues, although attempts to use computer algorithms relying on gene expression profiles, structural phenotyping, and statistical combination of structural and functional measurements have been proposed to allow reliable, quantitative comparison [44–46, 220]. The appropriate cell sources at the necessary seeding densities must be identified, customized bioreactors built, optimization of conditioning parameters established, and standards for desired tissue growth established before implantation can be attempted. This level of in vitro customization results in high cost and time to clinic for a tissue engineered scaffold [220–222], limiting the success of the process and product. Traditional tissue engineered scaffolds that are seeded with cells in vitro are evaluated by a number of biological parameters such as how the cells adhere to and penetrate the scaffold, what and when phenotypic changes occur, the metabolic activity of the cells/tissue, and how the cells/tissue function in vitro [108]. How these parameters change over time depends on the scaffold, cells, culture conditions, bioreactors, and time in culture which are unique to each application and are likely to change dramatically post implant. By focusing on cell-free scaffolds, we can apply well defined quality metrics to the scaffold itself [223, 224]. Scaffold qualities that include mechanics, biochemical composition, porosity, fiber alignment, three dimensional architecture, and cargo release profiles can be precisely and quantitatively measured. Fabricating cell-free scaffolds from the ground up (i.e. using as few biochemical components as are necessary) not only provides precisely measurable quality control metrics but also simplifies the host-response problem by narrowing the parameter space.

4.1 Heart Structure Following Injury or Disease

Scaffolds designed for cardiac repair aim to improve upon the body's limited endogenous repair mechanisms. Heart failure is often associated with tissue fibrosis and scarring [34] and fibrosis throughout the cardiovascular system leads to maladaptive remodeling and inefficient function of myocardial, valve, and vascular tissues. Fibrosis in the myocardium due to infarct can cause hypertrophic expansion of the ventricles leading to poor contractile efficiency and reduced cardiac output. Fibrosis of the cardiac valves can lead to calcification, resulting in stenosis and/or insufficiency and reduced cardiac output. Repairing and preventing the structural remodeling resulting from these pathological conditions

requires that synthetic scaffolds provide the biological cues necessary to direct cellular activity in a manner that inhibits or reverses scar formation.

Myofibroblasts are the primary ECM-secreting cells during wound healing and fibrosis [221]. The transition of fibroblasts to myofibroblasts is an early event in hypertensive heart disease and following myocardial infarction [34] that is regulated in part by mechanical tension and increased expression of renin-angiotensin-aldosterone (RAAS) hormones, endothelin-1, and transforming growth factor-β1 (TGF-β1) [5, 222]. Altered balance of matrix metalloproteinases (MMP)s and their inhibitors (tissue inhibitor MMP, TIMP) can stiffen the ECM [34], which is known to alter myocyte shape and contractile function [8]. Post-injury remodeling of the myocardium is associated with disrupted excitation-contraction coupling [34] and increased risk for arrhythmogenesis [223]. Functional restoration of cardiac tissues therefore requires strategies that regulate these factors and produce outcomes that are superior to scarring.

4.2 Fibrous Scaffolds for Myocardial Tissue Regeneration

Fibrous scaffolds have been designed for myocardial tissue engineering and patching to restore partial contractile function to infarcted ventricular myocardium. Many of these approaches support the benefit of using ECM-inspired nanofibrous scaffolds to mimic native tissue anisotropy and thereby enhance cell assembly into functional contractile myocardial tissues. Utilization of ECM proteins that are typically found in the native tissue is postulated to serve as a promising strategy for designing fibrous scaffolds optimized for myocardial repair. For example, Serpooshan et al. [224] demonstrated that an engineered acellular scaffold comprising type I collagen grafted onto the infarcted myocardium in adult murine hearts immediately after ligation of left anterior descending artery significantly protected the cardiac tissue from injury at the anatomical and functional levels. Patched ventricles showed attenuated left ventricular remodeling, diminished fibrosis, and formation of a network of interconnected blood vessels within the infarct (Table 10). These studies provide strong evidence that acellular biomaterials with ECM-like properties can modulate endogenous repair mechanisms and attenuate pathological remodeling to improve heart function following myocardial infarction.

Further efforts attempted to combine the cell-instructive capabilities of natural ECM proteins with the enhanced structural stability of biodegradable polymers to form so-called —bio-hybrid nanofibers. Electrospinning is the most widely used method for biohybrid cardiac patch production (Table 10) and several studies have demonstrated enhanced structure and function of engineered cardiac tissues by further doping the scaffold with electrically conductive materials [225, 226]. For example, Dvir et al. [225] observed improved contractile synchronicity in cardiac tissues that were grown in porous alginate scaffolds that contained gold nanowires compared to alginate scaffolds alone. More recently, Kharaziha et al. [226] reported stronger spontaneous and synchronous beating behavior (3.5-fold lower excitation threshold and 2.8-fold higher maximum capture rate) of cardiac tissues grown on aligned poly(-glycerol sebacate):gelatin (PG) electrospun nanofibrous scaffolds that contained carbon nanotubes compared to those cultured on PG scaffold alone. These

studies provide a glimpse into the potential that nanofibrous scaffolds have to serve as substrates as bioactive myocardial patches.

The use of cells and bioactive molecules to target endogenous repair mechanisms for cardiac repair was recently reviewed by Hastings et al. [227]. They noted that acellular material-based molecule delivery strategies do not require cell engraftment prior to implantation and can aid in clinical translation. They reviewed the potential to load small molecules such as prostaglandins and pyrvinium pamoate, RNA therapeutics, growth factors and proteins into biomaterial matrices provided that the release kinetics can be controlled. A variety of molecules have been successfully loaded into fiber scaffolds, including antibiotics and antibacterial agents, anticancer drugs, protein, DNA, RNA, and growth factors, and their release kinetics determined [228]. Drug release from electrospun fibers can be controlled by engineering nanofibers that undergo alterations in response to pH, temperature, light, electric fields, or combined stimuli [229]. The incorporation of these components into nanofiber scaffolds enhances cardiac repair by mitigating host rejection and promoting successful engraftment. For example, controlled delivery of FGF1 and neuregulin-1 growth factors promoted cardiac repair in a rat myocardial infarction model [230] and an angiogenic factor, FGF2, combined with an anti-inflammatory cytokine, interleukin-10, synergistically enhanced ischemic heart repair [231]. The incorporation of anti-inflammatory agents is an important consideration in the design of biomaterial scaffolds for therapeutic applications, but determining the most effective method to release the most relevant combination of factors is a continuing challenge [232].

Although electrospinning is the most commonly used method for nanofiber production, force extrusion is emerging as an alternative with a number of production advantages, such as higher throughput. For example, Bursac et al. [233] created aligned 3D polymer scaffolds by casting poly(lactic-co-glycolic) acid (PLGA) on extrusion-spun fibrous sucrose templates. They used a cotton candy machine to extrude sucrose fibers that were then manually stretched and pressed to form thin sheets. The sucrose templates were coated with PLGA solutions and the sucrose was leached out leaving PLGA scaffolds that were coated with fibronectin to promote cell adhesion to the scaffolds. Neonatal rat cardiac cells cultured on these scaffolds aligned and interconnected to form multiple bundles that exhibited anisotropic electrophysiological properties. Conduction velocity anisotropy ratios of 2 obtained after 2 weeks of culture were in agreement with those previously measured in neonatal ventricles. Given these early demonstrations of successful cardiac patch production and appreciating that force-spinning is a rapidly evolving technology platform [28, 29, 200], we expect these methods will be increasingly applied to myocardial tissue engineering.

4.3 Fibrous Scaffolds for Valve Replacement

In contrast to mechanical or bioprosthetic heart valves, fibrous constructs preserve multiscale features of natural valves and possess the ability to promote endogenous remodeling. These 3D fibrous valve scaffolds support cell culture and matrix remodeling in response to physiologically-relevant flows and pressures when cultured in vitro [240] or in vivo [241]. Implantation of non-endothelialized heart valve constructs into non-human primates resulted in nearly confluent endothelialization after just 4 weeks in vivo [242],

suggesting that endothelialization prior to implantation may not be necessary. This is important because reducing long-term *in vitro* culture and conditioning simplifies design and testing and reduces risk of infection. Engineered valve scaffolds that are either seeded with patient-derived stem cells or implanted cell-free may overcome the limitations of immunogenic rejection reported for xenogenic or allogenic transplants. Importantly, they are not dependent on the availability of healthy human donor tissue and may be tailored to patient-specific needs. This is especially true for cell-free scaffolds for which informed design, based on patient data, scaffold fabrication and implantation can be achieved in less than a day. It may also be possible to implant these scaffolds using minimally invasive procedures. For example, Weber et al. [240] confirmed that the structure of tissue engineered valves based on a synthetic biodegradable PGA/polyester composite matrix was not affected by crimping, suggesting the feasibility of stented, catheter implantation. Although further study is required to assess the long-term function of these scaffolds in vivo, mounting evidence suggests that cell-free or minimally tissue engineered personalized valve scaffolds can provide immediate functional restoration with the potential for in vivo remodeling and improved host integration.

5. Design Challenges and Future Directions

We began this review with the question *can we build a heart?* In order to provide a frame of reference for defining the aspects of heart function and disease that are being addressed using tissue engineering. Model cardiac tissue components that recapitulate portions of cardiac tissue structure and function have been engineered for both in vitro and in vivo applications. The design and build of these tissues are guided by what we observe and measure in the native tissue which likewise provides functional quality standards for their evaluation. The challenge moving forward is to establish goal-directed production based on clearly defined design criteria and benchmarks for success. To accomplish this, we must further define and determine scaling of the minimal, essential structures and functions of the native heart that need to be recapitulated. Tables such as those reported here instruct us on how to build cardiac tissue components as well as how to evaluate whole-organ function but we lack the understanding on how to translate between the two. Further, it is necessary to develop quantitative metrics that allow robust measurement and comparison of the parameters that define heart function. Computational algorithms allow quantitative assessment of traditionally qualitative measurements of biological form and function, such as calculation of global sarcomere alignment [45] or nuclear eccentricity [220] from fluorescence micrographs. Machine learning and statistical approaches for integrating the values from a variety of biochemical, structural, and functional experimental measurements into a single quality assessment score will allow comprehensive and reliable determination of engineered tissue quality [44, 46, 108]. As our knowledge of cardiac physiology grows, it would be of great utility to tabulate these data into a unified, digital repository that can be used to take a systems biology approach to defining comprehensive, clinically-relevant criteria for guiding the design of engineered cardiac tissues.

Despite advances in our knowledge of the structure and mechanics of the heart, and improvements in the materials and production methods used to manufacture synthetic scaffolds, post-implantation monitoring of scaffold remodeling and performance will be

challenging. Assessment of cell infiltration, scaffold degradation, degree of vascularization and remodeling can be accomplished with histological analysis following explantation. However, this type of analysis often requires termination of the growing scaffold/tissue complex. Real-time, nondestructive imaging and functional analysis methodologies capable of assessing engineered tissue performance in situ are needed to reveal the true time-dependent nature of the remodeling. Clinical diagnostic tools such as magnetic resonance imaging techniques (MRI) [225], computerized tomography (CT) [226], fluorescence imaging techniques [227], and echo/Doppler techniques may be useful to track scaffold/tissue growth and integration. Furthermore, fibrous scaffolds manufactured with dopants like magnetic or conductive nanoparticles can potentially be instrumented within the scaffold fibers during fabrication allowing for external, nondestructive monitoring of scaffold/tissue performance.

The need for vascularization strategies in tissue engineering was recognized early on [243] and remains a key challenge in the field [244–246]. The initiation of healthy angiogenesis has been and continues to be a primary concern for any implanted scaffold, from amorphous hydrogels [247] to highly aligned fibrous scaffolds. If, during the remodeling of the scaffold, angiogenesis is not initiated, the thickness of the tissue formed will be restricted to the diffusion limit of oxygen and nutrients from the surrounding vasculature (~200 μm thick) [245]. To overcome this, scaffolds such as those designed for cardiac or skeletal muscle that require substantial thickness will benefit from the inclusion of angiogenic growth factors or initiators such as vascular endothelial growth factor (VEGF) to promote endogenous vascularization [248–250]. However, thicker scaffolds will not only need to be chemically and biologically designed to initiate angiogenesis, but must also be physically designed to allow for vessel infiltration. The porosity of a fibrous scaffold is therefore a critical design parameter for supporting vascularization of engineered tissues. For thicker scaffolds designed for myocardial repair, high porosity will be crucial for long-term, full regeneration. However, for tissues such as cardiac valves that must remain thin to be optimally functional, a balance between porosity levels high enough for cell infiltration but low enough to prevent vascularization will need to be achieved.

A similar balance and tuning of scaffold biochemical and mechanical properties will likewise need to be achieved to initiate an ideal inflammatory host response that will eventually promote healthy tissue regeneration. Defining the —healthy level of inflammation is non-trivial: what is the minimal response to initiate endogenous tissue regeneration within the scaffold but not scarring or complete rejection? During the inflammatory phase of healing, matrix metalloproteinase (MMP) activation produces ECM fragments with potent pro-inflammatory actions affecting fibroblasts, endothelial cells, and leukocytes [42]. A key aim for cardiac regeneration strategies is the identification of signaling pathways that can be used to manage post-infarction inflammation, prevent excessive matrix degradation and attenuate adverse remodeling that leads to scar formation [251]. To accomplish this, anti-inflammatory, biologically-derived polymers [252] and synthetic anti-inflammatory drugs [253] have been incorporated directly into fibrous scaffolds. However, increasing the complexity of fibrous scaffolds by including more components, dopants, and cargo, may increase the risk for chronic inflammation and rejection. For example, instrumenting dopants such as conductive nanoparticles or

nanotubes may cause chronic inflammation or toxicity [254], likely dependent on where the scaffold is implanted. Controlling the inflammatory and angiogenic responses of the body are important design considerations of fibrous scaffolds moving forward and will require substantial investigation into the basic science of regenerative cellular processes. The advantage of using synthetically produced fibrous scaffolds compared to decellularized tissues is particularly evident here, as they are built from the bottom-up, adding only the components that are essential to a given application and can be thoroughly tested for their capacity to induce an immunological response.

In addition to these basic science design' challenges, the industrial manufacturability of fibrous tissue engineered products is an important, often overlooked consideration that continues to limit their translation to the clinic. Manufacturing scalability, storage, and shelf-life optimization, as well as, the establishment and implementation of quality control standards are hurdles for clinical translation and the development of reproducible in vitro assays. The importance of quality control and process validation, utilizing the scientific method to improve manufacturing process performance, was first proposed in the 1930s [255]. The implementation of statistics-based quality management practices over the decades since has led to substantial improvements in manufacturing efficiency and product quality in a wide range of manufacturing sectors because it provides insight about when a process is drifting out of control, a critical advantage over subjective, judgement-based assessment [256]. Statistical quality control inspection practices have been refined into a quality control paradigm commonly known as —Six Sigma that has been successfully utilized to minimize the occurrence of product defects by holding process variation to one-sixth the difference between process mean and the upper/lower design specification limits [256]. Multi-parameter statistical quality assessment strategies for stem cell manufacturing [45, 46] have already been implemented as well. We suggest the same can be done for fibrous tissue engineered products. Quantitative determination of standardized values for parameters such as fiber diameter, thickness, pore size, stiffness, and permeability similar to what is seen in decellularized ECM matrices (Table 9) will facilitate manufacturing and allow for standardized comparison. The adoption of these practices and standards will also accelerate products through the regulatory pathway if they are implemented early on in the development process. The translation of fibrous scaffolds into products with real patient impact will require a fusion of basic science and industrial manufacturing principles incorporated into the engineering design process.

6. Conclusion

In this review, we address the question, *can we build a heart?* Currently, mechanical ventricular assists and electronic pacemakers are able to restore the basic pumping functionality of the heart, and mechanical or fixed tissue valves can restore one-way flow functionality to damaged cardiac valves. However, prosthetic devices are only capable of sustaining basic function, and are not able to respond to dynamic changes in physiological demand. The heart is a living organ, capable of adapting its functional performance according to changing demands. By recapitulating the structure of the native heart using fibrous ECM scaffolds, it may be possible to build engineered heart tissues from cells that self-organize according to the guidance cues provided by the ECM into constructs capable

of the physiological profile of native heart tissues. Despite current limitations, we have begun to define the multi-scale, developmental, structural, and functional design criteria necessary to faithfully recapitulate the essential components of a working heart. Methods for mimicking the fibrous ECM of the myocardium, such as decellularized tissue, electrospinning, and force spinning, provide the manufacturing methods and materials to build heart parts with relevant compositions and architectures for both in vitro and in vivo applications. In vitro platforms based on engineered cardiac tissues will increasingly be used to discover therapeutics and tandem approaches to implantable devices will facilitate host integration. However, incorporating bioactive components within scaffolds to enhance their cell-instructive capabilities presents new challenges for safety and efficacy regulation when therapeutic applications are considered. Diverse roles played by the ECM in regulating thrombosis, inflammation, angiogenesis, and mediating interaction between multiple cell types are largely unexplored in these systems. Although valve replacement with fibrous scaffolds may be achieved in the short term, the use of these scaffolds for myocardial repair requires further study in vitro and in vivo. Further elucidation of the interactions between myocardial cells and bioartificial scaffolds will allow the fabrication of myocardial tissue models that can be more successfully applied to basic cardiology, and drug discovery. Although routine clinical use of engineered scaffolds for cardiac tissue repair has yet to be achieved, our ability to re-create the heart from engineered component parts is continually advancing.

Acknowledgments

References

1. Hench LL, Polak JM. Third-generation biomedical materials. Science. 2002; 295:1014–1017. [PubMed: 11834817]

2. Dabiri BE, Lee H, Parker KK. A potential role for integrin signaling in mechanoelectrical feedback. Progress in biophysics and molecular biology. 2012; 110:196–203. [PubMed: 22819851]

3. Frangogiannis NG. Matricellular proteins in cardiac adaptation and disease. Physiological reviews. 2012; 92:635–688. [PubMed: 22535894]

4. Bornstein P, Sage EH. Matricellular proteins: extracellular modulators of cell function. Current opinion in cell biology. 2002; 14:608–616. [PubMed: 12231357]

5. Dobaczewski M, Gonzalez-Quesada C, Frangogiannis NG. The extracellular matrix as a modulator of the inflammatory and reparative response following myocardial infarction. J Mol Cell Cardiol. 2010; 48:504–511. [PubMed: 19631653]

6. Chen JH, Simmons CA. Cell-matrix interactions in the pathobiology of calcific aortic valve disease: critical roles for matricellular, matricrine, and matrix mechanics cues. Circ Res. 2011; 108:1510–1524. [PubMed: 21659654]

7. Parker KK, Ingber DE. Extracellular matrix, mechanotransduction and structural hierarchies in heart tissue engineering. Philosophical transactions of the Royal Society of London. Series B Biological sciences. 2007; 362:1267–1279. [PubMed: 17588874]

8. McCain ML, Yuan H, Pasqualini FS, Campbell PH, Parker KK. Matrix elasticity regulates the optimal cardiac myocyte shape for contractility. American journal of physiology Heart and circulatory physiology. 2014; 306:H1525–1539. [PubMed: 24682394]

9. Grosberg A, Alford PW, McCain ML, Parker KK. Ensembles of engineered cardiac tissues for physiological and pharmacological study: heart on a chip. Lab Chip. 2011; 11:4165–4173. [PubMed: 22072288]

10. Feinberg AW, Alford PW, Jin H, Ripplinger CM, Werdich AA, Sheehy SP, Grosberg A, Parker KK. Controlling the contractile strength of engineered cardiac muscle by hierarchal tissue architecture. Biomaterials. 2012; 33:5732–5741. [PubMed: 22594976]

11. Sheehy SP, Grosberg A, Parker KK. The contribution of cellular mechanotransduction to cardiomyocyte form and function. Biomech Model Mechanobiol. 2012; 11:1227–1239. [PubMed: 22772714]

12. Harrison RG. The reaction of embryonic cells to solid structures. J Exp Zool. 1914; 17:521–544.

13. Weiss P. Experiments on cell and axon orientation in vitro; the role of colloidal exudates in tissue organization. J Exp Zool. 1945; 100:353–386. [PubMed: 21010856]

14. Dunn GA, Ebendal T. Contact guidance on oriented collagen gels. Experimental cell research. 1978; 111:475–479. [PubMed: 627251]

15. Curtis A, Wilkinson C. Topographical control of cells. Biomaterials. 1997; 18:1573–1583. [PubMed: 9613804]

16. Wang N, Butler JP, Ingber DE. Mechanotransduction across the Cell-Surface and through the Cytoskeleton. Science. 1993; 260:1124–1127. [PubMed: 7684161]

17. Gumbiner BM. Cell adhesion: the molecular basis of tissue architecture and morphogenesis. Cell. 1996; 84:345–357. [PubMed: 8608588]

18. Ingber DE. Mechanosensation through integrins: Cells act locally but think globally. Proceedings of the National Academy of Sciences of the United States of America. 2003; 100:1472–1474. [PubMed: 12578965]

19. Geiger B, Spatz JP, Bershadsky AD. Environmental sensing through focal adhesions. Nat Rev Mol Cell Bio. 2009; 10:21–33. [PubMed: 19197329]

20. Bosman FT, Stamenkovic I. Functional structure and composition of the extracellular matrix. The Journal of pathology. 2003; 200:423–428. [PubMed: 12845610]

21. Tsang KY, Cheung MC, Chan D, Cheah KS. The developmental roles of the extracellular matrix: beyond structure to regulation. Cell and tissue research. 2010; 339:93–110. [PubMed: 19885678]

22. Kim BS, Mooney DJ. Development of biocompatible synthetic extracellular matrices for tissue engineering. Trends in biotechnology. 1998; 16:224–230. [PubMed: 9621462]

23. Ma PX. Biomimetic materials for tissue engineering. Advanced drug delivery reviews. 2008; 60:184–198. [PubMed: 18045729]

24. Dvir T, Timko BP, Kohane DS, Langer R. Nanotechnological strategies for engineering complex tissues. Nat Nanotechnol. 2011; 6:13–22. [PubMed: 21151110]

25. Teo WE, Inai R, Ramakrishna S. Technological advances in electrospinning of nanofibers. Sci Technol Adv Mat. 2011; 12

26. Teo WE, Ramakrishna S. A review on electrospinning design and nanofibre assemblies. Nanotechnology. 2006; 17:R89–R106. [PubMed: 19661572]

27. Pham QP, Sharma U, Mikos AG. Electrospinning of polymeric nanofibers for tissue engineering applications: a review. Tissue engineering. 2006; 12:1197–1211. [PubMed: 16771634]

28. Badrossamay MR, McIlwee HA, Goss JA, Parker KK. Nanofiber assembly by rotary jet-spinning. Nano letters. 2010; 10:2257–2261. [PubMed: 20491499]

29. Badrossamay MR, Balachandran K, Capulli AK, Golecki HM, Agarwal A, Goss JA, Kim H, Shin K, Parker KK. Engineering hybrid polymer-protein super-aligned nanofibers via rotary jet spinning. Biomaterials. 2014; 35:3188–3197. [PubMed: 24456606]

30. Madurantakam PA, Cost CP, Simpson DG, Bowlin GL. Science of nanofibrous scaffold fabrication: strategies for next generation tissue-engineering scaffolds. Nanomedicine (Lond). 2009; 4:193–206. [PubMed: 19193185]

31. Bouten CV, Dankers PY, Driessen-Mol A, Pedron S, Brizard AM, Baaijens FP. Substrates for cardiovascular tissue engineering. Advanced drug delivery reviews. 2011; 63:221–241. [PubMed: 21277921]

32. Laflamme MA, Murry CE. Heart regeneration. Nature. 2011; 473:326–335. [PubMed: 21593865]

33. Frangogiannis NG, Smith CW, Entman ML. The inflammatory response in myocardial infarction. Cardiovascular research. 2002; 53:31–47. [PubMed: 11744011]

34. Berk BC, Fujiwara K, Lehoux S. ECM remodeling in hypertensive heart disease. J Clin Invest. 2007; 117:568–575. [PubMed: 17332884]

35. Patel CB, Cowger JA, Zuckermann A. A contemporary review of mechanical circulatory support. The Journal of heart and lung transplantation : the official publication of the International Society for Heart Transplantation. 2014; 33:667–674.

36. Wang G, McCain ML, Yang L, He A, Pasqualini FS, Agarwal A, Yuan H, Jiang D, Zhang D, Zangi L, Geva J, Roberts AE, Ma Q, Ding J, Chen J, Wang DZ, Li K, Wang J, Wanders RJ, Kulik W, Vaz FM, Laflamme MA, Murry CE, Chien KR, Kelley RI, Church GM, Parker KK, Pu WT. Modeling the mitochondrial cardiomyopathy of Barth syndrome with induced pluripotent stem cell and heart-on-chip technologies. Nature medicine. 2014; 20:616–623.

37. Benam KH, Dauth S, Hassell B, Herland A, Jain A, Jang KJ, Karalis K, Kim HJ, MacQueen L, Mahmoodian R, Musah S, Torisawa YS, van der Meer AD, Villenave R, Yadid M, Parker KK, Ingber DE. Engineered in vitro disease models. Annual review of pathology. 2015; 10:195–262.

38. Beltrami AP, Barlucchi L, Torella D, Baker M, Limana F, Chimenti S, Kasahara H, Rota M, Musso E, Urbanek K, Leri A, Kajstura J, Nadal-Ginard B, Anversa P. Adult cardiac stem cells are multipotent and support myocardial regeneration. Cell. 2003; 114:763–776. [PubMed: 14505575]

39. Hsieh PCH, Segers VFM, Davis ME, MacGillivray C, Gannon J, Molkentin JD, Robbins J, Lee RT. Evidence from a genetic fate-mapping study that stem cells refresh adult mammalian cardiomyocytes after injury. Nature medicine. 2007; 13:970–974.

40. Hong KU, Bolli R. Cardiac stem cell therapy for cardiac repair. Current treatment options in cardiovascular medicine. 2014; 16:324. [PubMed: 24903489]

41. Behfar A, Crespo-Diaz R, Terzic A, Gersh BJ. Cell therapy for cardiac repair--lessons from clinical trials. Nature reviews Cardiology. 2014; 11:232–246. [PubMed: 24594893]

42. Frangogiannis NG. Regulation of the inflammatory response in cardiac repair. Circ Res. 2012; 110:159–173. [PubMed: 22223212]

43. Bayomy AF, Bauer M, Qiu YL, Liao RL. Regeneration in heart disease-Is ECM the key? Life sciences. 2012; 91:823–827. [PubMed: 22982346]

44. Cahan P, Li H, Morris SA, Lummertz da Rocha E, Daley GQ, Collins JJ. CellNet: network biology applied to stem cell engineering. Cell. 2014; 158:903–915. [PubMed: 25126793]

45. Pasqualini FS, Sheehy SP, Agarwal A, Aratyn-Schaus Y, Parker KK. Structural Phenotyping of Stem Cell-Derived Cardiomyocytes. Stem cell reports. 2015; 4:340–347. [PubMed: 25733020]

46. Sheehy SP, Pasqualini F, Grosberg A, Park SJ, Aratyn-Schaus Y, Parker KK. Quality Metrics for Stem Cell-Derived Cardiac Myocytes. Stem cell reports. 2014; 2:282–294. [PubMed: 24672752]

47. Kocica MJ, Corno AF, Carreras-Costa F, Ballester-Rodes M, Moghbel MC, Cueva CN, Lackovic V, Kanjuh VI, Torrent-Guasp F. The helical ventricular myocardial band: global, three-dimensional, functional architecture of the ventricular myocardium. European journal of cardio-thoracic surgery : official journal of the European Association for Cardio-thoracic Surgery. 2006; 29(Suppl 1):S21–40. [PubMed: 16563790]

48. Fleischer S, Dvir T. Tissue engineering on the nanoscale: lessons from the heart. Curr Opin Biotech. 2013; 24:664–671. [PubMed: 23142543]

49. Robinson TF, Geraci MA, Sonnenblick EH, Factor SM. Coiled perimysial fibers of papillary muscle in rat heart: morphology, distribution, and changes in configuration. Circ Res. 1988; 63:577–592. [PubMed: 3409489]

50. Pope AJ, Sands GB, Smaill BH, LeGrice IJ. Three-dimensional transmural organization of perimysial collagen in the heart. American journal of physiology Heart and circulatory physiology. 2008; 295:H1243–H1252. [PubMed: 18641274]

51. Savadjiev P, Strijkers GJ, Bakermans AJ, Piuze E, Zucker SW, Siddiqi K. Heart wall myofibers are arranged in minimal surfaces to optimize organ function. Proceedings of the National Academy of Sciences of the United States of America. 2012; 109:9248–9253. [PubMed: 22645368]

52. Mammoto T, Mammoto A, Ingber DE. Mechanobiology and developmental control. Annu Rev Cell Dev Biol. 2013; 29:27–61. [PubMed: 24099083]

53. Sheehy SP, Parker KK. The Role of Mechanical Forces in Guiding Tissue Differentiation. Stem Cells Biol Reg. 2011:77–97.

54. Ingber DE, Wang N, Stamenovic D. Tensegrity, cellular biophysics, and the mechanics of living systems. Rep Prog Phys. 2014; 77:046603. [PubMed: 24695087]

55. Grosberg A, Kuo PL, Guo CL, Geisse NA, Bray MA, Adams WJ, Sheehy SP, Parker KK. Self-organization of muscle cell structure and function. PLoS Comput Biol. 2011; 7:e1001088. [PubMed: 21390276]

56. Geisse NA, Sheehy SP, Parker KK. Control of myocyte remodeling in vitro with engineered substrates. In Vitro Cell Dev Biol Anim. 2009; 45:343–350. [PubMed: 19252956]

57. Kuo PL, Lee H, Bray MA, Geisse NA, Huang YT, Adams WJ, Sheehy SP, Parker KK. Myocyte shape regulates lateral registry of sarcomeres and contractility. The American journal of pathology. 2012; 181:2030–2037. [PubMed: 23159216]

58. Samarel AM. Costameres, focal adhesions, and cardiomyocyte mechanotransduction. American journal of physiology Heart and circulatory physiology. 2005; 289:H2291–2301. [PubMed: 16284104]

59. Sequeira V, Nijenkamp LL, Regan JA, van der Velden J. The physiological role of cardiac cytoskeleton and its alterations in heart failure. Biochimica et biophysica acta. 2014; 1838:700–722. [PubMed: 23860255]

60. Harvey PA, Leinwand LA. Cellular mechanisms of cardiomyopathy. Journal of Cell Biology. 2011; 194:355–365. [PubMed: 21825071]

61. McCain ML, Parker KK. Mechanotransduction: the role of mechanical stress, myocyte shape, and cytoskeletal architecture on cardiac function. Pflugers Archiv : European journal of physiology. 2011; 462:89–104. [PubMed: 21499986]

62. Huang S, Ingber DE. Shape-dependent control of cell growth, differentiation, and apoptosis: switching between attractors in cell regulatory networks. Experimental cell research. 2000; 261:91–103. [PubMed: 11082279]

63. Danowski BA, Imanaka-Yoshida K, Sanger JM, Sanger JW. Costameres are sites of force transmission to the substratum in adult rat cardiomyocytes. The Journal of cell biology. 1992; 118:1411–1420. [PubMed: 1522115]

64. Hoshijima M. Mechanical stress-strain sensors embedded in cardiac cytoskeleton: Z disk, titin, and associated structures. American journal of physiology Heart and circulatory physiology. 2006; 290:H1313–1325. [PubMed: 16537787]

65. Russell B, Curtis MW, Koshman YE, Samarel AM. Mechanical stress-induced sarcomere assembly for cardiac muscle growth in length and width. J Mol Cell Cardiol. 2010; 48:817–823. [PubMed: 20188736]

66. McCain ML, Lee H, Aratyn-Schaus Y, Kleber AG, Parker KK. Cooperative coupling of cell-matrix and cell-cell adhesions in cardiac muscle. Proceedings of the National Academy of Sciences of the United States of America. 2012; 109:9881–9886. [PubMed: 22675119]

67. Lee H, Adams WJ, Alford PW, McCain ML, Feinberg AW, Sheehy SP, Goss JA, Parker KK. Cytoskeletal prestress regulates nuclear shape and stiffness in cardiac myocytes. Exp Biol Med (Maywood). 2015

68. Sheehy SP, Huang S, Parker KK. Time-warped comparison of gene expression in adaptive and maladaptive cardiac hypertrophy. Circ Cardiovasc Genet. 2009; 2:116–124. [PubMed: 20031575]

69. Decker ML, Simpson DG, Behnke M, Cook MG, Decker RS. Morphological analysis of contracting and quiescent adult rabbit cardiac myocytes in long-term culture. Anat Rec. 1990; 227:285–299. [PubMed: 2372136]

70. Majkut S, Idema T, Swift J, Krieger C, Liu A, Discher DE. Heart-specific stiffening in early embryos parallels matrix and myosin expression to optimize beating. Curr Biol. 2013; 23:2434–2439. [PubMed: 24268417]

71. Christoffels VM, Pu WT. Developing insights into cardiac regeneration. Development. 2013; 140:3933–3937. [PubMed: 24046314]

72. Bergmann O, Bhardwaj RD, Bernard S, Zdunek S, Barnabe-Heider F, Walsh S, Zupicich J, Alkass K, Buchholz BA, Druid H, Jovinge S, Frisen J. Evidence for Cardiomyocyte Renewal in Humans. Science. 2009; 324:98–102. [PubMed: 19342590]

73. Mollova M, Bersell K, Walsh S, Savla J, Das LT, Park SY, Silberstein LE, dos Remedios CG, Graham D, Colan S, Kuhn B. Cardiomyocyte proliferation contributes to heart growth in young humans. Proceedings of the National Academy of Sciences of the United States of America. 2013; 110:1446–1451. [PubMed: 23302686]

74. Muralidhar SA, Mahmoud AI, Canseco D, Xiao F, Sadek HA. Harnessing the power of dividing cardiomyocytes. Global cardiology science & practice. 2013; 2013:212–221. [PubMed: 24689023]

75. Hall, JE. Guyton and Hall textbook of medical physiology. 13. Elsevier; Philadelphia, PA: 2016.

76. Rosen MR, Brink PR, Cohen IS, Robinson RB. Cardiac pacing: from biological to electronic ... to biological? Circulation Arrhythmia and electrophysiology. 2008; 1:54–61. [PubMed: 19808394]

77. Rosen MR, Robinson RB, Brink PR, Cohen IS. The road to biological pacing. Nature reviews Cardiology. 2011; 8:656–666. [PubMed: 21844918]

78. Hu YF, Dawkins JF, Cho HC, Marban E, Cingolani E. Biological pacemaker created by minimally invasive somatic reprogramming in pigs with complete heart block. Science translational medicine. 2014; 6:245ra294.

79. Chauveau S, Brink PR, Cohen IS. Stem cell-based biological pacemakers from proof of principle to therapy: a review. Cytotherapy. 2014; 16:873–880. [PubMed: 24831844]

80. Arrenberg AB, Stainier DY, Baier H, Huisken J. Optogenetic control of cardiac function. Science. 2010; 330:971–974. [PubMed: 21071670]

81. Bruegmann T, Malan D, Hesse M, Beiert T, Fuegemann CJ, Fleischmann BK, Sasse P. Optogenetic control of heart muscle in vitro and in vivo. Nature methods. 2010; 7:897–900. [PubMed: 20881965]

82. Bingen BO, Engels MC, Schalij MJ, Jangsangthong W, Neshati Z, Feola I, Ypey DL, Askar SF, Panfilov AV, Pijnappels DA, de Vries AA. Light-induced termination of spiral wave arrhythmias by optogenetic engineering of atrial cardiomyocytes. Cardiovascular research. 2014; 104:194–205. [PubMed: 25082848]

83. Ambrosi CM, Klimas A, Yu J, Entcheva E. Cardiac applications of optogenetics. Progress in biophysics and molecular biology. 2014; 115:294–304. [PubMed: 25035999]

84. Kleber AG, Rudy Y. Basic mechanisms of cardiac impulse propagation and associated arrhythmias. Physiological reviews. 2004; 84:431–488. [PubMed: 15044680]

85. Glukhov AV, Fedorov VV, Kalish PW, Ravikumar VK, Lou Q, Janks D, Schuessler RB, Moazami N, Efimov IR. Conduction remodeling in human end-stage nonischemic left ventricular cardiomyopathy. Circulation. 2012; 125:1835–1847. [PubMed: 22412072]

86. Caldwell BJ, Trew ML, Sands GB, Hooks DA, LeGrice IJ, Smaill BH. Three distinct directions of intramural activation reveal nonuniform side-to-side electrical coupling of ventricular myocytes. Circulation Arrhythmia and electrophysiology. 2009; 2:433–440. [PubMed: 19808500]

87. Hooks DA, Tomlinson KA, Marsden SG, LeGrice IJ, Smaill BH, Pullan AJ, Hunter PJ. Cardiac microstructure: implications for electrical propagation and defibrillation in the heart. Circ Res. 2002; 91:331–338. [PubMed: 12193466]

88. Katz AM. Ernest Henry Starling, his predecessors, and the "Law of the Heart". Circulation. 2002; 106:2986–2992. [PubMed: 12460884]

89. Granzier HL, Irving TC. Passive tension in cardiac muscle: contribution of collagen, titin, microtubules, and intermediate filaments. Biophysical journal. 1995; 68:1027–1044. [PubMed: 7756523]

90. Granzier HL, Labeit S. The giant protein titin: a major player in myocardial mechanics, signaling, and disease. Circ Res. 2004; 94:284–295. [PubMed: 14976139]

91. Irving TC, Konhilas J, Perry D, Fischetti R, De Tombe PP. Myofilament lattice spacing as a function of sarcomere length in isolated rat myocardium. Am J Physiol-Heart C. 2000; 279:H2568–H2573.

92. Hanft LM, McDonald KS. Sarcomere length dependence of power output is increased after PKA treatment in rat cardiac myocytes. Am J Physiol-Heart C. 2009; 296:H1524–H1531.

93. McDonald KS. The interdependence of Ca2+ activation, sarcomere length, and power output in the heart. Pflugers Archiv : European journal of physiology. 2011; 462:61–67. [PubMed: 21404040]

94. Ait Mou Y, le Guennec JY, Mosca E, de Tombe PP, Cazorla O. Differential contribution of cardiac sarcomeric proteins in the myofibrillar force response to stretch. Pflugers Archiv : European journal of physiology. 2008; 457:25–36. [PubMed: 18449562]

95. de Tombe PP, Mateja RD, Tachampa K, Ait Mou Y, Farman GP, Irving TC. Myofilament length dependent activation. J Mol Cell Cardiol. 2010; 48:851–858. [PubMed: 20053351]

96. Shiels HA, White E. The Frank-Starling mechanism in vertebrate cardiac myocytes. J Exp Biol. 2008; 211:2005–2013. [PubMed: 18552289]

97. Iribe G, Helmes M, Kohl P. Force-length relations in isolated intact cardiomyocytes subjected to dynamic changes in mechanical load. American journal of physiology Heart and circulatory physiology. 2007; 292:H1487–1497. [PubMed: 17098830]

98. Bollensdorff C, Lookin O, Kohl P. Assessment of contractility in intact ventricular cardiomyocytes using the dimensionless 'Frank-Starling Gain' index. Pflugers Archiv : European journal of physiology. 2011; 462:39–48. [PubMed: 21494804]

99. Methawasin M, Hutchinson KR, Lee EJ, Smith JE 3rd, Saripalli C, Hidalgo CG, Ottenheijm CA, Granzier H. Experimentally increasing titin compliance in a novel mouse model attenuates the Frank-Starling mechanism but has a beneficial effect on diastole. Circulation. 2014; 129:1924–1936. [PubMed: 24599837]

100. Wilders R. Arrhythmogenic right ventricular cardiomyopathy: considerations from in silico experiments. Front Physiol. 2012; 3:168. [PubMed: 22754532]

101. McCain ML, Desplantez T, Geisse NA, Rothen-Rutishauser B, Oberer H, Parker KK, Kleber AG. Cell-to-cell coupling in engineered pairs of rat ventricular cardiomyocytes: relation between Cx43 immunofluorescence and intercellular electrical conductance. American journal of physiology Heart and circulatory physiology. 2012; 302:H443–450. [PubMed: 22081700]

102. Burkhoff D, Mirsky I, Suga H. Assessment of systolic and diastolic ventricular properties via pressure-volume analysis: a guide for clinical, translational, and basic researchers. American journal of physiology Heart and circulatory physiology. 2005; 289:H501–512. [PubMed: 16014610]

103. Kolipaka A, Araoz PA, Mcgee KP, Manduca A, Ehman RL. Magnetic Resonance Elastography as a Method for the Assessment of Effective Myocardial Stiffness Throughout the Cardiac Cycle. Magnetic resonance in medicine. 2010; 64:862–870. [PubMed: 20578052]

104. Chen CH, Fetics B, Nevo E, Rochitte CE, Chiou KR, Ding PA, Kawaguchi M, Kass DA. Noninvasive single-beat determination of left ventricular end-systolic elastance in humans. Journal of the American College of Cardiology. 2001; 38:2028–2034. [PubMed: 11738311]

105. Gayat E, Mor-Avi V, Weinert L, Yodwut C, Lang RM. Noninvasive quantification of left ventricular elastance and ventricular-arterial coupling using three-dimensional echocardiography and arterial tonometry. American journal of physiology Heart and circulatory physiology. 2011; 301:H1916–1923. [PubMed: 21908790]

106. Chaturvedi RR, Herron T, Simmons R, Shore D, Kumar P, Sethia B, Chua F, Vassiliadis E, Kentish JC. Passive stiffness of myocardium from congenital heart disease and implications for diastole. Circulation. 2010; 121:979–988. [PubMed: 20159832]

107. Zhang KW, French B, May Khan A, Plappert T, Fang JC, Sweitzer NK, Borlaug BA, Chirinos JA, St John Sutton M, Cappola TP, Ky B. Strain improves risk prediction beyond ejection fraction in chronic systolic heart failure. Journal of the American Heart Association. 2014; 3:e000550. [PubMed: 24419736]

108. Yang X, Pabon L, Murry CE. Engineering adolescence: maturation of human pluripotent stem cell-derived cardiomyocytes. Circ Res. 2014; 114:511–523. [PubMed: 24481842]

109. Turnbull IC, Karakikes I, Serrao GW, Backeris P, Lee JJ, Xie C, Senyei G, Gordon RE, Li RA, Akar FG, Hajjar RJ, Hulot JS, Costa KD. Advancing functional engineered cardiac tissues toward a preclinical model of human myocardium. Faseb J. 2014; 28:644–654. [PubMed: 24174427]

110. Rossman EI, Petre RE, Chaudhary KW, Piacentino V 3rd, Janssen PM, Gaughan JP, Houser SR, Margulies KB. Abnormal frequency-dependent responses represent the pathophysiologic signature of contractile failure in human myocardium. J Mol Cell Cardiol. 2004; 36:33–42. [PubMed: 14734045]

111. Lundy SD, Zhu WZ, Regnier M, Laflamme MA. Structural and functional maturation of cardiomyocytes derived from human pluripotent stem cells. Stem Cells Dev. 2013; 22:1991–2002. [PubMed: 23461462]

112. Drouin E, Charpentier F, Gauthier C, Laurent K, Le Marec H. Electrophysiologic characteristics of cells spanning the left ventricular wall of human heart: evidence for presence of M cells. Journal of the American College of Cardiology. 1995; 26:185–192. [PubMed: 7797750]

113. Poveda F, Gil D, Marti E, Andaluz A, Ballester M, Carreras F. Helical Structure of the Cardiac Ventricular Anatomy Assessed by Diffusion Tensor Magnetic Resonance Imaging With Multiresolution Tractography. Revista espanola de cardiologia. 2013; 66:782–790. [PubMed: 24773858]

114. Goktepe S, Abilez OJ, Parker KK, Kuhl E. A multiscale model for eccentric and concentric cardiac growth through sarcomerogenesis. J Theor Biol. 2010; 265:433–442. [PubMed: 20447409]

115. Otto, CM. Valvular heart disease. W.B. Saunders; Philadelphia: 1999.

116. Williams C, Quinn KP, Georgakoudi I, Black LD 3rd. Young developmental age cardiac extracellular matrix promotes the expansion of neonatal cardiomyocytes in vitro. Acta biomaterialia. 2014; 10:194–204. [PubMed: 24012606]

117. Anderson KP, Walker R, Urie P, Ershler PR, Lux RL, Karwandee SV. Myocardial Electrical Propagation in Patients with Idiopathic Dilated Cardiomyopathy. J Clin Invest. 1993; 92:122–140. [PubMed: 8325977]

118. Kleber AG, Janse MJ, Wilms-Schopmann FJ, Wilde AA, Coronel R. Changes in conduction velocity during acute ischemia in ventricular myocardium of the isolated porcine heart. Circulation. 1986; 73:189–198. [PubMed: 3940667]

119. Rossi S, Baruffi S, Bertuzzi A, Miragoli M, Corradi D, Maestri R, Alinovi R, Mutti A, Musso E, Sgoifo A, Brisinda D, Fenici R, Macchi E. Ventricular activation is impaired in aged rat hearts. Am J Physiol-Heart C. 2008; 295:H2336–H2347.

120. Fast VG, Kleber AG. Anisotropic conduction in monolayers of neonatal rat heart cells cultured on collagen substrate. Circ Res. 1994; 75:591–595. [PubMed: 8062430]

121. Bursac N, Parker KK, Iravanian S, Tung L. Cardiomyocyte cultures with controlled macroscopic anisotropy: a model for functional electrophysiological studies of cardiac muscle. Circ Res. 2002; 91:e45–54. [PubMed: 12480825]

122. Liau B, Christoforou N, Leong KW, Bursac N. Pluripotent stem cell-derived cardiac tissue patch with advanced structure and function. Biomaterials. 2011; 32:9180–9187. [PubMed: 21906802]

123. Zhang D, Shadrin IY, Lam J, Xian HQ, Snodgrass HR, Bursac N. Tissue-engineered cardiac patch for advanced functional maturation of human ESC-derived cardiomyocytes. Biomaterials. 2013; 34:5813–5820. [PubMed: 23642535]

124. Wenk JF, Klepach D, Lee LC, Zhang Z, Ge L, Tseng EE, Martin A, Kozerke S, Gorman JH 3rd, Gorman RC, Guccione JM. First evidence of depressed contractility in the border zone of a human myocardial infarction. The Annals of thoracic surgery. 2012; 93:1188–1193. [PubMed: 22326127]

125. Kissling G, Gassenmaier T, Wendt-Gallitelli MF, Jacob R. Pressure-volume relations, elastic modulus, and contractile behaviour of the hypertrophied left ventricle of rats with Goldblatt II hypertension. Pflugers Archiv : European journal of physiology. 1977; 369:213–221. [PubMed: 142962]

126. Gosselin H, Qi X, Rouleau JL. Correlation between cardiac remodelling, function, and myocardial contractility in rat hearts 5 weeks after myocardial infarction. Can J Physiol Pharm. 1998; 76:53–62.

127. Hasenfuss G, Mulieri LA, Blanchard EM, Holubarsch C, Leavitt BJ, Ittleman F, Alpert NR. Energetics of isometric force development in control and volume-overload human myocardium. Comparison with animal species. Circ Res. 1991; 68:836–846. [PubMed: 1742869]

128. Agarwal A, Goss JA, Cho A, McCain ML, Parker KK. Microfluidic heart on a chip for higher throughput pharmacological studies. Lab Chip. 2013; 13:3599–3608. [PubMed: 23807141]

129. Nishimura S, Yasuda S, Katoh M, Yamada KP, Yamashita H, Saeki Y, Sunagawa K, Nagai R, Hisada T, Sugiura S. Single cell mechanics of rat cardiomyocytes under isometric, unloaded, and physiologically loaded conditions. American journal of physiology Heart and circulatory physiology. 2004; 287:H196–202. [PubMed: 15001443]

130. Wassenaar PA, Eleswarpu CN, Schroeder SA, Mo X, Raterman BD, White RD, Kolipaka A. Measuring age-dependent myocardial stiffness across the cardiac cycle using MR elastography: A reproducibility study. Magnetic resonance in medicine. 2015

131. Mirsky I, Tajimi T, Peterson KL. The Development of the Entire End-Systolic Pressure-Volume and Ejection Fraction Afterload Relations - a New Concept of Systolic Myocardial Stiffness. Circulation. 1987; 76:343–356. [PubMed: 3608122]

132. Clark NR, Reichek N, Bergey P, Hoffman EA, Brownson D, Palmon L, Axel L. Circumferential myocardial shortening in the normal human left ventricle. Assessment by magnetic resonance imaging using spatial modulation of magnetization. Circulation. 1991; 84:67–74. [PubMed: 2060124]

133. Moore CC, Lugo-Olivieri CH, McVeigh ER, Zerhouni EA. Three-dimensional systolic strain patterns in the normal human left ventricle: characterization with tagged MR imaging. Radiology. 2000; 214:453–466. [PubMed: 10671594]

134. Ingels NB Jr, Daughters GT 2nd, Stinson EB, Alderman EL. Measurement of midwall myocardial dynamics in intact man by radiography of surgically implanted markers. Circulation. 1975; 52:859–867. [PubMed: 1175267]

135. Kim DH, Lipke EA, Kim P, Cheong R, Thompson S, Delannoy M, Suh KY, Tung L, Levchenko A. Nanoscale cues regulate the structure and function of macroscopic cardiac tissue constructs. Proceedings of the National Academy of Sciences of the United States of America. 2010; 107:565–570. [PubMed: 20018748]

136. Qu F, Ripplinger CM, Nikolski VP, Grimm C, Efimov IR. Three-dimensional panoramic imaging of cardiac arrhythmias in rabbit heart. Journal of biomedical optics. 2007; 12:044019. [PubMed: 17867823]

137. Weiwad WK, Linke WA, Wussling MH. Sarcomere length-tension relationship of rat cardiac myocytes at lengths greater than optimum. J Mol Cell Cardiol. 2000; 32:247–259. [PubMed: 10722801]

138. Tracqui P, Ohayon J. An integrated formulation of anisotropic force-calcium relations driving spatio-temporal contractions of cardiac myocytes. Philos T R Soc A. 2009; 367:4887–4905.

139. Aikawa E, Whittaker P, Farber M, Mendelson K, Padera RF, Aikawa M, Schoen FJ. Human semilunar cardiac valve remodeling by activated cells from fetus to adult: implications for postnatal adaptation, pathology, and tissue engineering. Circulation. 2006; 113:1344–1352. [PubMed: 16534030]

140. Rajamannan NM, Evans FJ, Aikawa E, Grande-Allen KJ, Demer LL, Heistad DD, Simmons CA, Masters KS, Mathieu P, O'Brien KD, Schoen FJ, Towler DA, Yoganathan AP, Otto CM. Calcific Aortic Valve Disease: Not Simply a Degenerative Process A Review and Agenda for Research From the National Heart and Lung and Blood Institute Aortic Stenosis Working Group. Circulation. 2011; 124:1783–1791. [PubMed: 22007101]

141. Dweck MR, Boon NA, Newby DE. Calcific aortic stenosis: a disease of the valve and the myocardium. Journal of the American College of Cardiology. 2012; 60:1854–1863. [PubMed: 23062541]

142. Sacks MS, Yoganathan AP. Heart valve function: a biomechanical perspective. Philos T R Soc B. 2007; 362:1369–1391.

143. Vesely I. Heart valve tissue engineering. Circ Res. 2005; 97:743–755. [PubMed: 16224074]

144. Marom G, Peleg M, Halevi R, Rosenfeld M, Raanani E, Hamdan A, Haj-Ali R. Fluid-structure interaction model of aortic valve with porcine-specific collagen fiber alignment in the cusps. Journal of biomechanical engineering. 2013; 135:101001–101006. [PubMed: 23775457]

145. Hinton RB Jr, Lincoln J, Deutsch GH, Osinska H, Manning PB, Benson DW, Yutzey KE. Extracellular matrix remodeling and organization in developing and diseased aortic valves. Circ Res. 2006; 98:1431–1438. [PubMed: 16645142]

146. Butcher JT, Mahler GJ, Hockaday LA. Aortic valve disease and treatment: the need for naturally engineered solutions. Advanced drug delivery reviews. 2011; 63:242–268. [PubMed: 21281685]

147. Brinkley DM, Gelfand EV. Valvular heart disease: classic teaching and emerging paradigms. The American journal of medicine. 2013; 126:1035–1042. [PubMed: 24125637]

148. Hutcheson JD, Aikawa E, Merryman WD. Potential drug targets for calcific aortic valve disease. Nature reviews Cardiology. 2014; 11:218–231. [PubMed: 24445487]

149. Liu AC, Joag VR, Gotlieb AI. The emerging role of valve interstitial cell phenotypes in regulating heart valve pathobiology. The American journal of pathology. 2007; 171:1407–1418. [PubMed: 17823281]

150. Yip CYY, Simmons CA. The aortic valve microenvironment and its role in calcific aortic valve disease. Cardiovascular Pathology. 2011; 20:177–182. [PubMed: 21256052]

151. Chen MB, Srigunapalan S, Wheeler AR, Simmons CA. A 3D microfluidic platform incorporating methacrylated gelatin hydrogels to study physiological cardiovascular cell-cell interactions. Lab Chip. 2013; 13:2591–2598. [PubMed: 23525275]

152. Wylie-Sears J, Aikawa E, Levine RA, Yang JH, Bischoff J. Mitral Valve Endothelial Cells With Osteogenic Differentiation Potential. Arterioscl Throm Vas. 2011; 31:598–U266.

153. Werner N, Kosiol S, Schiegl T, Ahlers P, Walenta K, Link A, Bohm M, Nickenig G. Circulating endothelial progenitor cells and cardiovascular outcomes. New Engl J Med. 2005; 353:999–1007. [PubMed: 16148285]

154. Huang HY, Huang S. Real-time strain mapping via biaxial stretching in heart valve tissues. Conference proceedings : ... Annual International Conference of the IEEE Engineering in Medicine and Biology Society IEEE Engineering in Medicine and Biology Society Annual Conference. 2012; 2012:6653–6656.

155. Schoen FJ. Mechanisms of function and disease of natural and replacement heart valves. Annual review of pathology. 2012; 7:161–183.

156. Otto CM. Evaluation and management of chronic mitral regurgitation. New Engl J Med. 2001; 345:740–746. [PubMed: 11547744]

157. Thomas L, Foster E, Schiller NB. Peak mitral inflow velocity predicts mitral regurgitation severity. Journal of the American College of Cardiology. 1998; 31:174–179. [PubMed: 9426037]

158. Dohmen PM, Lembcke A, Hotz H, Kivelitz D, Konertz WF. Ross operation with a tissue-engineered heart valve. The Annals of thoracic surgery. 2002; 74:1438–1442. [PubMed: 12440590]

159. Baumgartner H, Hung J, Bermejo J, Chambers JB, Evangelista A, Griffin BP, Iung B, Otto CM, Pellikka PA, Quinones M. Eae/Ase, Echocardiographic assessment of valve stenosis: EAE/ASE recommendations for clinical practice. European journal of echocardiography : the journal of the Working Group on Echocardiography of the European Society of Cardiology. 2009; 10:1–25.

160. Sacks MS, Enomoto Y, Graybill JR, Merryman WD, Zeeshan A, Yoganathan AP, Levy RJ, Gorman RC, Gorman JH 3rd. In-vivo dynamic deformation of the mitral valve anterior leaflet. The Annals of thoracic surgery. 2006; 82:1369–1377. [PubMed: 16996935]

161. Sacks MS, David Merryman W, Schmidt DE. On the biomechanics of heart valve function. Journal of biomechanics. 2009; 42:1804–1824. [PubMed: 19540499]

162. Yap CH, Saikrishnan N, Yoganathan AP. Experimental measurement of dynamic fluid shear stress on the ventricular surface of the aortic valve leaflet. Biomech Model Mechanobiol. 2012; 11:231–244. [PubMed: 21465260]

163. Schenke-Layland K, Riemann I, Opitz F, Konig K, Halbhuber KJ, Stock UA. Comparative study of cellular and extracellular matrix composition of native and tissue engineered heart valves.

Matrix biology : journal of the International Society for Matrix Biology. 2004; 23:113–125. [PubMed: 15246110]

164. Song JJ, Ott HC. Organ engineering based on decellularized matrix scaffolds. Trends in molecular medicine. 2011; 17:424–432. [PubMed: 21514224]

165. Del Gaudio C, Bianco A, Grigioni M. Electrospun bioresorbable trileaflet heart valve prosthesis for tissue engineering: in vitro functional assessment of a pulmonary cardiac valve design. Annali dell'Istituto superiore di sanita. 2008; 44:178–186.

166. Badylak SF, Taylor D, Uygun K. Whole-Organ Tissue Engineering: Decellularization and Recellularization of Three-Dimensional Matrix Scaffolds. Annu Rev Biomed Eng. 2011; 13:27–53. [PubMed: 21417722]

167. Crapo PM, Gilbert TW, Badylak SF. An overview of tissue and whole organ decellularization processes. Biomaterials. 2011; 32:3233–3243. [PubMed: 21296410]

168. Fu RH, Wang YC, Liu SP, Shih TR, Lin HL, Chen YM, Sung JH, Lu CH, Wei JR, Wang ZW, Huang SJ, Tsai CH, Shyu WC, Lin SZ. Decellularization and Recellularization Technologies in Tissue Engineering. Cell transplantation. 2014; 23:621–630. [PubMed: 24816454]

169. Nichols JE, Niles J, Riddle M, Vargas G, Schilagard T, Ma L, Edward K, La Francesca S, Sakamoto J, Vega S, Ogadegbe M, Mlcak R, Deyo D, Woodson L, McQuitty C, Lick S, Beckles D, Melo E, Cortiella J. Production and Assessment of Decellularized Pig and Human Lung Scaffolds. Tissue Eng Pt A. 2013; 19:2045–2062.

170. Song JJ, Guyette JP, Gilpin SE, Gonzalez G, Vacanti JP, Ott HC. Regeneration and experimental orthotopic transplantation of a bioengineered kidney. Nature medicine. 2013; 19:646–651.

171. Akhyari P, Aubin H, Gwanmesia P, Barth M, Hoffmann S, Huelsmann J, Preuss K, Lichtenberg A. The Quest for an Optimized Protocol for Whole-Heart Decellularization: A Comparison of Three Popular and a Novel Decellularization Technique and Their Diverse Effects on Crucial Extracellular Matrix Qualities. Tissue Eng Part C-Me. 2011; 17:915–926.

172. Grayson WL, Frohlich M, Yeager K, Bhumiratana S, Chan ME, Cannizzaro C, Wan LQ, Liu XS, Guo XE, Vunjak-Novakovic G. Engineering anatomically shaped human bone grafts. Proceedings of the National Academy of Sciences of the United States of America. 2010; 107:3299–3304. [PubMed: 19820164]

173. Bertanha M, Moroz A, Almeida R, Alves FC, Valerio MJA, Moura R, Domingues MAC, Sobreira ML, Deffune E. Tissue-engineered blood vessel substitute by reconstruction of endothelium using mesenchymal stem cells induced by platelet growth factors. J Vasc Surg. 2014; 59:1677–1685. [PubMed: 23830317]

174. Guyette JP, Gilpin SE, Charest JM, Tapias LF, Ren X, Ott HC. Perfusion decellularization of whole organs. Nat Protoc. 2014; 9:1451–1468. [PubMed: 24874812]

175. Ott HC, Matthiesen TS, Goh SK, Black LD, Kren SM, Netoff TI, Taylor DA. Perfusion-decellularized matrix: using nature's platform to engineer a bioartificial heart. Nature medicine. 2008; 14:213–221.

176. Lu TY, Lin B, Kim J, Sullivan M, Tobita K, Salama G, Yang L. Repopulation of decellularized mouse heart with human induced pluripotent stem cell-derived cardiovascular progenitor cells. Nat Commun. 2013; 4

177. Badylak SF. Decellularized Allogeneic and Xenogeneic Tissue as a Bioscaffold for Regenerative Medicine: Factors that Influence the Host Response. Annals of biomedical engineering. 2014; 42:1517–1527. [PubMed: 24402648]

178. Keane TJ, Londono R, Turner NJ, Badylak SF. Consequences of ineffective decellularization of biologic scaffolds on the host response. Biomaterials. 2012; 33:1771–1781. [PubMed: 22137126]

179. Braghirolli DI, Steffens D, Pranke P. Electrospinning for regenerative medicine: a review of the main topics. Drug discovery today. 2014; 19:743–753. [PubMed: 24704459]

180. He JH, Kong HY, Yang RR, Dou H, Faraz N, Wang L, Feng C. Review on Fiber Morphology Obtained by Bubble Electrospinning and Blown Bubble Spinning. Therm Sci. 2012; 16:1263–1279.

181. Srivastava Y, Marquez M, Thorsen T. Microfluidic electrospinning of biphasic nanofibers with Janus morphology. Biomicrofluidics. 2009; 3

182. Nuansing W, Frauchiger D, Huth F, Rebollo A, Hillenbrand R, Bittner AM. Electrospinning of peptide and protein fibres: approaching the molecular scale. Faraday Discuss. 2013; 166:209–221.

183. Meng LH, Arnoult O, Smith M, Wnek GE. Electrospinning of in situ crosslinked collagen nanofibers. J Mater Chem. 2012; 22:19412–19417.

184. Fu W, Liu ZL, Feng B, Hu RJ, He XM, Wang H, Yin M, Huang HM, Zhang HB, Wang W. Electrospun gelatin/PCL and collagen/PLCL scaffolds for vascular tissue engineering. Int J Nanomed. 2014; 9:2335–2344.

185. Sell SA, McClure MJ, Garg K, Wolfe PS, Bowlin GL. Electrospinning of collagen/biopolymers for regenerative medicine and cardiovascular tissue engineering. Advanced drug delivery reviews. 2009; 61:1007–1019. [PubMed: 19651166]

186. Vasita R, Katti DS. Nanofibers and their applications in tissue engineering. Int J Nanomed. 2006; 1:15–30.

187. Fridrikh SV, Yu JH, Brenner MP, Rutledge GC. Controlling the fiber diameter during electrospinning. Phys Rev Lett. 2003; 90

188. Nam J, Huang Y, Agarwal S, Lannutti J. Improved cellular infiltration in electrospun fiber via engineered porosity. Tissue engineering. 2007; 13:2249–2257. [PubMed: 17536926]

189. Van Lieshout MI, Vaz CM, Rutten MCM, Peters GWM, Baaijens FPT. Electrospinning versus knitting: two scaffolds for tissue engineering of the aortic valve. J Biomat Sci-Polym E. 2006; 17:77–89.

190. Beachley V, Wen XJ. Effect of electrospinning parameters on the nanofiber diameter and length. Mat Sci Eng C-Bio S. 2009; 29:663–668.

191. Cui WG, Zhou Y, Chang J. Electrospun nanofibrous materials for tissue engineering and drug delivery. Sci Technol Adv Mat. 2010; 11

192. Ji W, Sun Y, Yang F, van den Beucken JJJP, Fan MW, Chen Z, Jansen JA. Bioactive Electrospun Scaffolds Delivering Growth Factors and Genes for Tissue Engineering Applications. Pharm Res-Dordr. 2011; 28:1259–1272.

193. Kai D, Prabhakaran MP, Jin GR, Ramakrishna S. Biocompatibility evaluation of electrically conductive nanofibrous scaffolds for cardiac tissue engineering. J Mater Chem B. 2013; 1:2305–2314.

194. Li Y, Fu JJ, Chen RS, Huang M, Gao B, Huo KF, Wang L, Chu PK. Core-shell TiC/C nanofiber arrays decorated with copper nanoparticles for high performance non-enzymatic glucose sensing. Sensor Actuat B-Chem. 2014; 192:474–479.

195. Lee HJ, Kim HS, Kim HO, Koh WG. Micropatterns of double-layered nanofiber scaffolds with dual functions of cell patterning and metabolite detection. Lab Chip. 2011; 11:2849–2857. [PubMed: 21738946]

196. Luo CJ, Stoyanov SD, Stride E, Pelan E, Edirisinghe M. Electrospinning versus fibre production methods: from specifics to technological convergence. Chem Soc Rev. 2012; 41:4708–4735. [PubMed: 22618026]

197. Chase GG, Varabhas JS, Reneker DH. New Methods to Electrospin Nanofibers. J Eng Fiber Fabr. 2011; 6:32–38.

198. Zeugolis DI, Khew ST, Yew ESY, Ekaputra AK, Tong YW, Yung LYL, Hutmacher DW, Sheppard C, Raghunath M. Electro-spinning of pure collagen nano-fibres - Just an expensive way to make gelatin? Biomaterials. 2008; 29:2293–2305. [PubMed: 18313748]

199. Hutmacher DW, Dalton PD. Melt Electrospinning. Chem-Asian J. 2011; 6:44–56. [PubMed: 21080400]

200. Mellado P, McIlwee HA, Badrossamay MR, Goss JA, Mahadevan L, Parker KK. A simple model for nanofiber formation by rotary jet-spinning. Appl Phys Lett. 2011; 99

201. Deravi L, Golecki HM, Parker KK. Protein-based textiles: bio-inspired and bio-derived materials for medical and non-medical applications. Journal of Chemical and Biological Interfaces. 2013; 1:25–34.

202. Sarkar K, Gomez C, Zambrano S, Ramirez M, de Hoyos E, Vasquez H, Lozano K. Electrospinning to Forcespinning (TM). Mater Today. 2010; 13:12–14.

203. Wang B, Tedder ME, Perez CE, Wang G, de Jongh Curry AL, To F, Elder SH, Williams LN, Simionescu DT, Liao J. Structural and biomechanical characterizations of porcine myocardial extracellular matrix. Journal of materials science Materials in medicine. 2012; 23:1835–1847. [PubMed: 22584822]

204. Wang B, Borazjani A, Tahai M, Curry AL, Simionescu DT, Guan J, To F, Elder SH, Liao J. Fabrication of cardiac patch with decellularized porcine myocardial scaffold and bone marrow mononuclear cells. Journal of biomedical materials research Part A. 2010; 94:1100–1110. [PubMed: 20694977]

205. Luo J, Korossis SA, Wilshaw SP, Jennings LM, Fisher J, Ingham E. Development and characterization of acellular porcine pulmonary valve scaffolds for tissue engineering. Tissue engineering Part A. 2014; 20:2963–2974. [PubMed: 24786313]

206. Lu Q, Ganesan K, Simionescu DT, Vyavahare NR. Novel porous aortic elastin and collagen scaffolds for tissue engineering. Biomaterials. 2004; 25:5227–5237. [PubMed: 15110474]

207. Ott HC, Matthiesen TS, Goh SK, Black LD, Kren SM, Netoff TI, Taylor DA. Perfusion-decellularized matrix: using nature's platform to engineer a bioartificial heart. Nature medicine. 2008; 14:213–221.

208. Shevach M, Fleischer S, Shapira A, Dvir T. Gold Nanoparticle-Decellularized Matrix Hybrids for Cardiac Tissue Engineering. Nano letters. 2014; 14:5792–5796. [PubMed: 25176294]

209. Rajabi-Zeleti S, Jalili-Firoozinezhad S, Azarnia M, Khayyatan F, Vandat S, Nikeghbalian S, Khademhosseini A, Baharvand H, Aghdami N. The behavior of cardiac progenitor cells on macroporous pericardium-derived scaffolds. Biomaterials. 2014; 35:970–982. [PubMed: 24183165]

210. Sanchez PL, Fernandez-Santos ME, Costanza S, Climent AM, Moscoso I, Gonzalez-Nicolas MA, Sanz-Ruiz R, Rodriguez H, Kren SM, Garrido G, Escalante JL, Bermejo J, Elizaga J, Menarguez J, Yotti R, del Villar CP, Espinosa MA, Guillem MS, Willerson JT, Bernad A, Matesanz R, Taylor DA, Fernandez-Aviles F. Acellular human heart matrix: A critical step toward whole heart grafts. Biomaterials. 2015; 61:279–289. [PubMed: 26005766]

211. Yu J, Lee AR, Lin WH, Lin CW, Wu YK, Tsai WB. Electrospun PLGA fibers incorporated with functionalized biomolecules for cardiac tissue engineering. Tissue engineering Part A. 2014; 20:1896–1907. [PubMed: 24471778]

212. Senel Ayaz HG, Perets A, Ayaz H, Gilroy KD, Govindaraj M, Brookstein D, Lelkes PI. Textile-templated electrospun anisotropic scaffolds for regenerative cardiac tissue engineering. Biomaterials. 2014; 35:8540–8552. [PubMed: 25017096]

213. Fleischer S, Feiner R, Shapira A, Ji J, Sui X, Daniel Wagner H, Dvir T. Spring-like fibers for cardiac tissue engineering. Biomaterials. 2013; 34:8599–8606. [PubMed: 23953840]

214. Rai R, Tallawi M, Frati C, Falco A, Gervasi A, Quaini F, Roether JA, Hochburger T, Schubert DW, Seik L, Barbani N, Lazzeri L, Rosellini E, Boccaccini AR. Bioactive Electrospun Fibers of Poly(glycerol sebacate), Poly(epsilon-caprolactone) for Cardiac Patch Application, Advanced healthcare materials. 2015

215. Masoumi N, Larson BL, Annabi N, Kharaziha M, Zamanian B, Shapero KS, Cubberley AT, Camci-Unal G, Manning KB, Mayer JE Jr, Khademhosseini A. Electrospun PGS:PCL microfibers align human valvular interstitial cells and provide tunable scaffold anisotropy. Advanced healthcare materials. 2014; 3:929–939. [PubMed: 24453182]

216. Hobson CM, Amoroso NJ, Amini R, Ungchusri E, Hong Y, D'Amore A, Sacks MS, Wagner WR. Fabrication of elastomeric scaffolds with curvilinear fibrous structures for heart valve leaflet engineering. Journal of biomedical materials research. Part A. 2015; 103:3101–3106. [PubMed: 25771748]

217. Hinderer S, Seifert J, Votteler M, Shen N, Rheinlaender J, Schaffer TE, Schenke-Layland K. Engineering of a bio-functionalized hybrid off-the-shelf heart valve. Biomaterials. 2014; 35:2130–2139. [PubMed: 24333025]

218. Zhang DM, Chang J. Electrospinning of Three-Dimensional Nanofibrous Tubes with Controllable Architectures. Nano letters. 2008; 8:3283–3287. [PubMed: 18767890]

219. Argento G, Simonet M, Oomens CW, Baaijens FP. Multi-scale mechanical characterization of scaffolds for heart valve tissue engineering. Journal of biomechanics. 2012; 45:2893–2898. [PubMed: 22999107]

220. Jones TR, Carpenter AE, Lamprecht MR, Moffat J, Silver SJ, Grenier JK, Castoreno AB, Eggert US, Root DE, Golland P, Sabatini DM. Scoring diverse cellular morphologies in image-based screens with iterative feedback and machine learning. Proceedings of the National Academy of Sciences of the United States of America. 2009; 106:1826–1831. [PubMed: 19188593]

221. Klingberg F, Hinz B, White ES. The myofibroblast matrix: implications for tissue repair and fibrosis. The Journal of pathology. 2013; 229:298–309. [PubMed: 22996908]

222. van den Borne SW, Diez J, Blankesteijn WM, Verjans J, Hofstra L, Narula J. Myocardial remodeling after infarction: the role of myofibroblasts. Nature reviews Cardiology. 2010; 7:30–37. [PubMed: 19949426]

223. Rohr S. Myofibroblasts in diseased hearts: new players in cardiac arrhythmias? Heart rhythm : the official journal of the Heart Rhythm Society. 2009; 6:848–856. [PubMed: 19467515]

224. Serpooshan V, Zhao M, Metzler SA, Wei K, Shah PB, Wang A, Mahmoudi M, Malkovskiy AV, Rajadas J, Butte MJ, Bernstein D, Ruiz-Lozano P. The effect of bioengineered acellular collagen patch on cardiac remodeling and ventricular function post myocardial infarction. Biomaterials. 2013; 34:9048–9055. [PubMed: 23992980]

225. Dvir T, Timko BP, Brigham MD, Naik SR, Karajanagi SS, Levy O, Jin H, Parker KK, Langer R, Kohane DS. Nanowired three-dimensional cardiac patches. Nat Nanotechnol. 2011; 6:720–725. [PubMed: 21946708]

226. Kharaziha M, Shin SR, Nikkhah M, Topkaya SN, Masoumi N, Annabi N, Dokmeci MR, Khademhosseini A. Tough and flexible CNT-polymeric hybrid scaffolds for engineering cardiac constructs. Biomaterials. 2014; 35:7346–7354. [PubMed: 24927679]

227. Hastings CL, Roche ET, Ruiz-Hernandez E, Schenke-Layland K, Walsh CJ, Duffy GP. Drug and cell delivery for cardiac regeneration. Advanced drug delivery reviews. 2015; 84:85–106. [PubMed: 25172834]

228. Hu X, Liu S, Zhou G, Huang Y, Xie Z, Jing X. Electrospinning of polymeric nanofibers for drug delivery applications. Journal of controlled release : official journal of the Controlled Release Society. 2014; 185:12–21. [PubMed: 24768792]

229. Weng L, Xie J. Smart electrospun nanofibers for controlled drug release: recent advances and new perspectives. Current pharmaceutical design. 2015; 21:1944–1959. [PubMed: 25732665]

230. Formiga FR, Pelacho B, Garbayo E, Imbuluzqueta I, Diaz-Herraez P, Abizanda G, Gavira JJ, Simon-Yarza T, Albiasu E, Tamayo E, Prosper F, Blanco-Prieto MJ. Controlled delivery of fibroblast growth factor-1 and neuregulin-1 from biodegradable microparticles promotes cardiac repair in a rat myocardial infarction model through activation of endogenous regeneration. Journal of controlled release : official journal of the Controlled Release Society. 2014; 173:132–139. [PubMed: 24200746]

231. Chen WC, Lee BG, Park DW, Kim K, Chu H, Kim K, Huard J, Wang Y. Controlled dual delivery of fibroblast growth factor-2 and Interleukin-10 by heparin-based coacervate synergistically enhances ischemic heart repair. Biomaterials. 2015; 72:138–151. [PubMed: 26370927]

232. Browne S, Pandit A. Biomaterial-mediated modification of the local inflammatory environment. Frontiers in bioengineering and biotechnology. 2015; 3:67. [PubMed: 26029692]

233. Bursac N, Loo Y, Leong K, Tung L. Novel anisotropic engineered cardiac tissues: studies of electrical propagation. Biochemical and biophysical research communications. 2007; 361:847–853. [PubMed: 17689494]

234. Zong XH, Bien H, Chung CY, Yin LH, Fang DF, Hsiao BS, Chu B, Entcheva E. Electrospun fine-textured scaffolds for heart tissue constructs. Biomaterials. 2005; 26:5330–5338. [PubMed: 15814131]

235. Kenar H, Kose GT, Toner M, Kaplan DL, Hasirci V. A 3D aligned microfibrous myocardial tissue construct cultured under transient perfusion. Biomaterials. 2011; 32:5320–5329. [PubMed: 21570112]

236. Kai D, Wang QL, Wang HJ, Prabhakaran MP, Zhang Y, Tan YZ, Ramakrishna S. Stem cell-loaded nanofibrous patch promotes the regeneration of infarcted myocardium with functional improvement in rat model. Acta biomaterialia. 2014; 10:2727–2738. [PubMed: 24576580]

237. Guex AG, Frobert A, Valentin J, Fortunato G, Hegemann D, Cook S, Carrel TP, Tevaearai HT, Giraud MN. Plasma-functionalized electrospun matrix for biograft development and cardiac function stabilization. Acta biomaterialia. 2014; 10:2996–3006. [PubMed: 24531014]

238. Chen QZ, Bismarck A, Hansen U, Junaid S, Tran MQ, Harding SE, Ali NN, Boccaccini AR. Characterisation of a soft elastomer poly(glycerol sebacate) designed to match the mechanical properties of myocardial tissue. Biomaterials. 2008; 29:47–57. [PubMed: 17915309]

239. Kang K, Sun L, Xiao Y, Li SH, Wu J, Guo J, Jiang SL, Yang L, Yau TM, Weisel RD, Radisic M, Li RK. Aged human cells rejuvenated by cytokine enhancement of biomaterials for surgical ventricular restoration. Journal of the American College of Cardiology. 2012; 60:2237–2249. [PubMed: 23153846]

240. Weber B, Robert J, Ksiazek A, Wyss Y, Frese L, Slamecka J, Kehl D, Modregger P, Peter S, Stampanoni M, Proulx S, Falk V, Hoerstrup SP. Living-engineered valves for transcatheter venous valve repair. Tissue engineering. Part C Methods. 2014; 20:451–463. [PubMed: 24156382]

241. Ghazanfari S, Driessen-Mol A, Sanders B, Dijkman PE, Hoerstrup SP, Baaijens FP, Bouten CV. In Vivo Collagen Remodeling in the Vascular Wall of Decellularized Stented Tissue-Engineered Heart Valves. Tissue engineering Part A. 2015; 21:2206–2215. [PubMed: 26028124]

242. Weber B, Scherman J, Emmert MY, Gruenenfelder J, Verbeek R, Bracher M, Black M, Kortsmit J, Franz T, Schoenauer R, Baumgartner L, Brokopp C, Agarkova I, Wolint P, Zund G, Falk V, Zilla P, Hoerstrup SP. Injectable living marrow stromal cell-based autologous tissue engineered heart valves: first experiences with a one-step intervention in primates. Eur Heart J. 2011; 32:2830–2840. [PubMed: 21415068]

243. Langer R, Vacanti JP. Tissue engineering. Science. 1993; 260:920–926. [PubMed: 8493529]

244. Lovett M, Lee K, Edwards A, Kaplan DL. Vascularization Strategies for Tissue Engineering. Tissue Eng Part B-Re. 2009; 15:353–370.

245. Novosel EC, Kleinhans C, Kluger PJ. Vascularization is the key challenge in tissue engineering. Advanced drug delivery reviews. 2011; 63:300–311. [PubMed: 21396416]

246. Baiguera S, Ribatti D. Endothelialization approaches for viable engineered tissues. Angiogenesis. 2013; 16:1–14. [PubMed: 23010872]

247. Drury JL, Mooney DJ. Hydrogels for tissue engineering: scaffold design variables and applications. Biomaterials. 2003; 24:4337–4351. [PubMed: 12922147]

248. Rujitanaroj PO, Aid-Launais R, Chew SY, Le Visage C. Polysaccharide electrospun fibers with sulfated poly(fucose) promote endothelial cell migration and VEGF-mediated angiogenesis. Biomater Sci-Uk. 2014; 2:843–852.

249. Miyagi Y, Chiu LL, Cimini M, Weisel RD, Radisic M, Li RK. Biodegradable collagen patch with covalently immobilized VEGF for myocardial repair. Biomaterials. 2011; 32:1280–1290. [PubMed: 21035179]

250. Chiu LL, Radisic M. Scaffolds with covalently immobilized VEGF and Angiopoietin-1 for vascularization of engineered tissues. Biomaterials. 2010; 31:226–241. [PubMed: 19800684]

251. Dobaczewski M, Xia Y, Bujak M, Gonzalez-Quesada C, Frangogiannis NG. CCR5 Signaling Suppresses Inflammation, Reduces Adverse Remodeling of the Infarcted Heart, Mediating Recruitment of Regulatory T Cells. American Journal of Pathology. 2010; 176:2177–2187. [PubMed: 20382703]

252. Merrell JG, McLaughlin SW, Tie L, Laurencin CT, Chen AF, Nair LS. Curcumin-loaded poly(epsilon-caprolactone) nanofibres: diabetic wound dressing with anti-oxidant and anti-inflammatory properties. Clinical and experimental pharmacology & physiology. 2009; 36:1149–1156. [PubMed: 19473187]

253. Kenawy ER, Abdel-Hay FI, El-Newehy MH, Wnek GE. Controlled release of ketoprofen from electrospun poly(vinyl alcohol) nanofibers. Mat Sci Eng a-Struct. 2007; 459:390–396.

254. Nel A, Xia T, Madler L, Li N. Toxic potential of materials at the nanolevel. Science. 2006; 311:622–627. [PubMed: 16456071]

255. Shewhart, WA.; Deming, WE. Statistical method from the viewpoint of quality control. The Graduate school, the Department of agriculture; Washington: 1939.

256. Hinckley CM. Defining the best quality-control systems by design and inspection. Clinical chemistry. 1997; 43:873–879. [PubMed: 9166256]
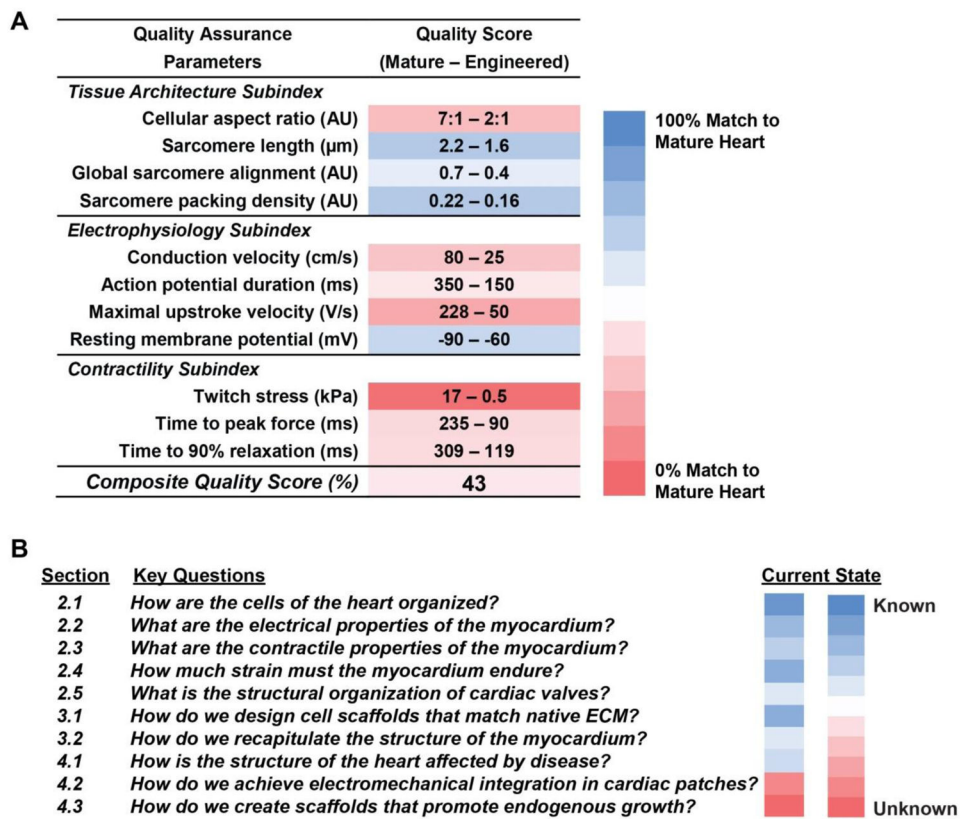
Fig. 1.

Quality assessment of engineered tissues. (A) Integration of a combination of structural and functional experimental measurements provides insight into the ability of engineered human stem cell-derived heart tissues to meet design criteria established according to —gold standard measurements made on mature heart tissues. Calculating a composite quality score by averaging the percent differences between the mature and engineered tissue measurement values could allow comprehensive quantitative comparison [108–112]. (B) To build engineered heart constructs, there are several key questions concerning design aspects that we address in this review.
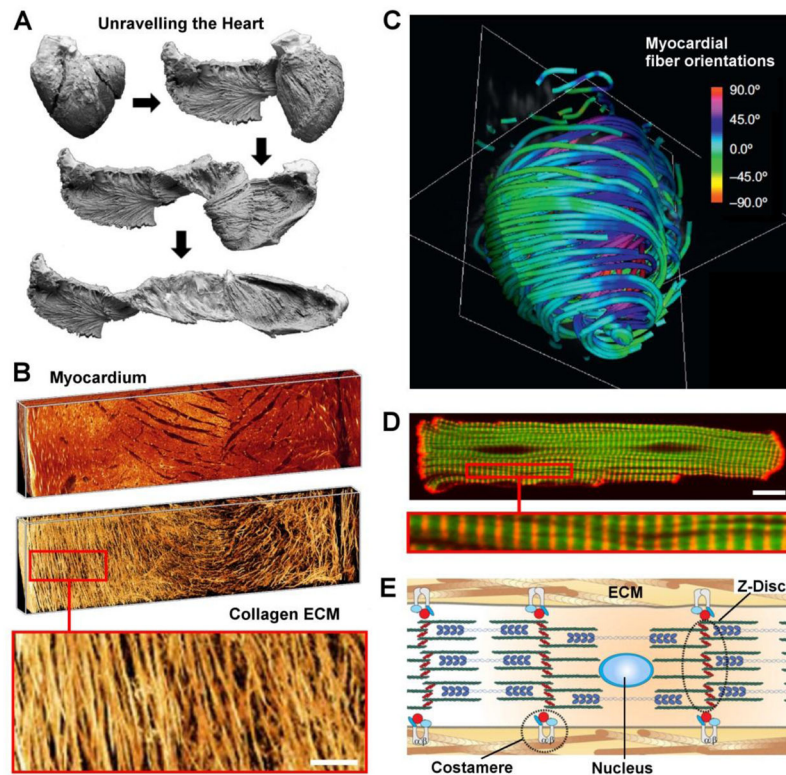
Fig. 2.

Multiscale structure of the myocardium. (A) Key phases of a dissection procedure (bovine heart) revealing the laminar architecture of the heart. Reprinted from [47] with permission from Elsevier; (B) Three-dimensional volume renderings of myocardial muscle (top) and collagen structures (bottom) extracted from images of Wistar-Kyoto rat left ventricles (LVs). Inset show fibrillar collagen structure, scale bar = 100 μm. Reprinted from [50] with permission from the American Physiological Society. (C) Color map of myocradial fiber orientation obtained using diffusion tensor magnetic resonance imaging (DTI). Full-color scheme represents fiber orientations, simplified tractography is shown. Adapted from [113] with permission from Elsevier; (D) Confocal fluorescence image of a cardiomyocyte: F-actin (green), α-actinin (red), magnified inset shows sarcomeric striations, scale bar = 10 μm. Reprinted from [114] with permission from Elsevier; (E) Schematic depicting cardiac myofibril organization in vivo. Integrins colocalized to the costamere help mechanically couple the intracellular z-disc to the extra-cellular matrix (ECM). Z-discs anchor the contractile actin-myosin machinery. Adjacent myocytes are coupled to each other via adherens junctions. Reprinted from [2] with permission from Elsevier.
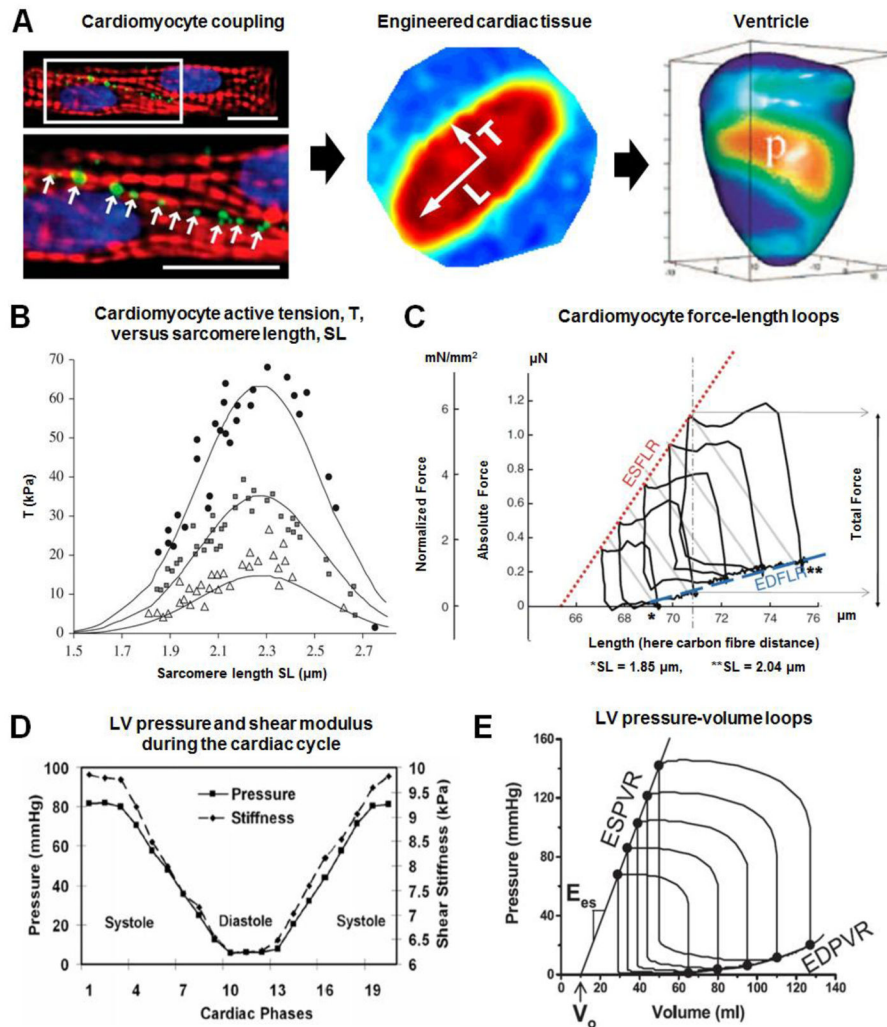
Fig. 3.

Multiscale electromechanical properties of the myocardium. (A) Left: Coupling between cardiomyocytes through specialized gap junctions (green: Cx43, red: actin, blue: nuclei). Adapted from [101] with permission from the National Academy of Sciences; Middle: anisotropic conduction in a patterned engineered cardiac tissue construct. Reprinted from [135] with permission from the National Academy of Sciences; Epicardial action potential texture mapping during epicardial pacing of a rabbit heart at location, p. Adapted from [136] with permission from the international society for optics and photonics; (B) Mechano-chemical couplings driving cardiomyocyte contraction modelled in silico (solid lines), fitting experimental data obtained by Weiwad et al. [137], highlighting the SL-active tension relationship for skinned cardiac cells activated in solutions with increasing Ca^{2+} concentrations. Filled circles, pCa=4.9; filled squares, pCa=5.46; open triangles, pCa=5.7. Reprinted from [138] with permission from the Royal Society; (C) Diagram representing end-diastolic and end-systolic force–length relations (EDFLR and ESFLR, respectively) of a Guinea pig intact isolated ventricular cardiomyocyte. The EDFLR (dashed line, blue) is obtained by monitoring passive tension (force required to arrive at different pre-loads),

while ESFLR (dotted line, red) is constructed by recording total force at the end of contractions, initiated from a range of different pre-loads (here covering a sarcomere length, SL, range from 1.85 to 2.05 μm). Reprinted from [98] with permission from Springer; (D) Plots of time-dependent ventricular pressure and stiffness during the cardiac cycle, measured in a healthy adult pig's left ventricle. The myocardium is stiffer in systole than in diastole. Reprinted from [103] with permission from Wiley; (E) Use of intra-ventricular pressure-volume loops to estimate the end-systolic pressure-volume relationship (ESPVR). The linear ESPVR is characterized by a slope (E_{es}) and a volume axis intercept (V_o). In contrast, the diastolic pressure-volume points define a nonlinear end-diastolic pressure/volume relationship (EDPVR). Reprinted from [102] with permission from the American Physiological Society.
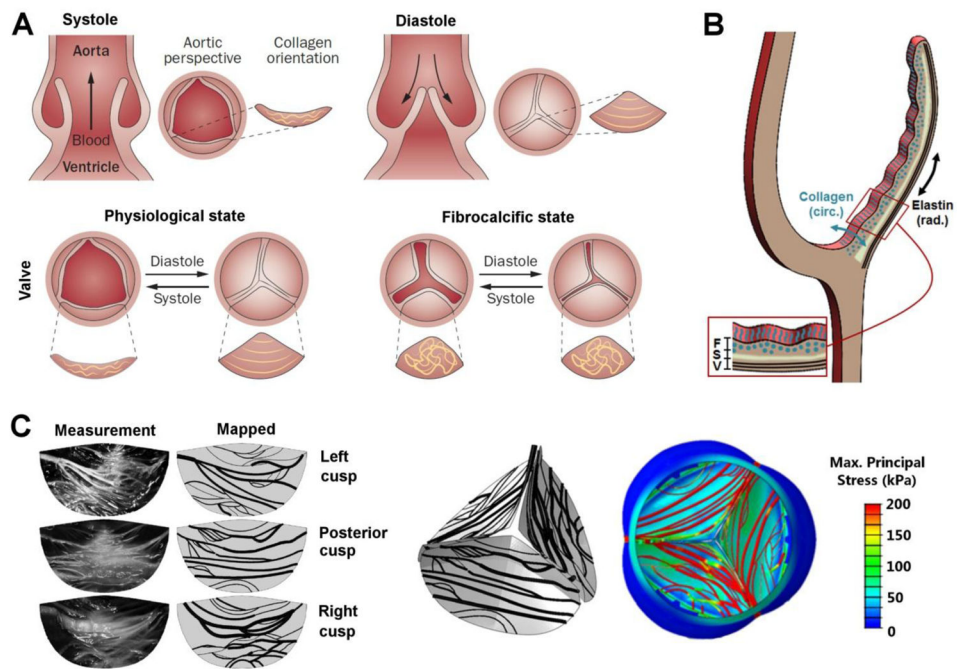
Fig. 4.
Structure of the aortic valve in health and disease. (A) Schematic description of a healthy aortic valve. Systolic contraction of the left ventricle forces the aortic valve leaflets to open, allowing blood to enter the aorta. The reversed pressure gradient, created when the heart rests in diastole, causes the aortic valve leaflets to close, preventing retrograde blood flow into the heart. Circumferential collagen alignment allows the leaflets to stretch in the radial direction while providing the tensile strength required to prevent leaflet prolapse. Loss of ECM organization associated with fibrocalcific diseased state. Reprinted from[148] with permission from Macmillan Publishers Limited; (B) Schematic cross-sectional view of a valve leaflet showing fibrosa, F, spongiosa, S, and ventricularis, V, layers. Circumferential collagen alignment in the fibrosa and radial elastin alignment in the ventricularis are indicated; (C) Left: Stretched cusps and the mapped collagen fiber network. Right: A 3D view from the aortic side of collagen fiber maps and associated maximum principal stress contours plotted on the deformed structure during diastole. Reprinted from[144] with permission from ASME.
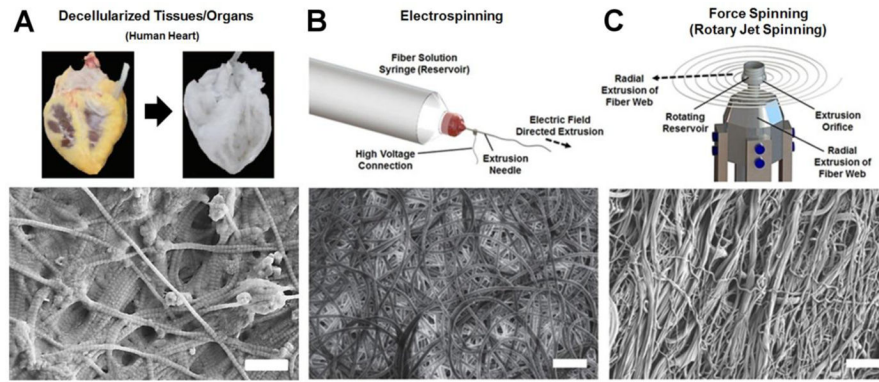
Fig. 5.
Strategies for building fibrous scaffolds. (A)Decellularized human heart (top), reprinted from [164] with permission from Elsevier, and decellularized porcine submucosa (bottom), scale bar is 500nm. (B) Electrospun fibrous use high voltages to extrude conductive fiber precursors, scale bar is 30μm, reprinted from [165] with permission from Istituto Superiore di Sanità. (C) Force spinning methods such as rotary jet spinning adopt many of the benefits of electrospinning while scaling up production levels and expanding material diversity, scale bar is 30 μm.
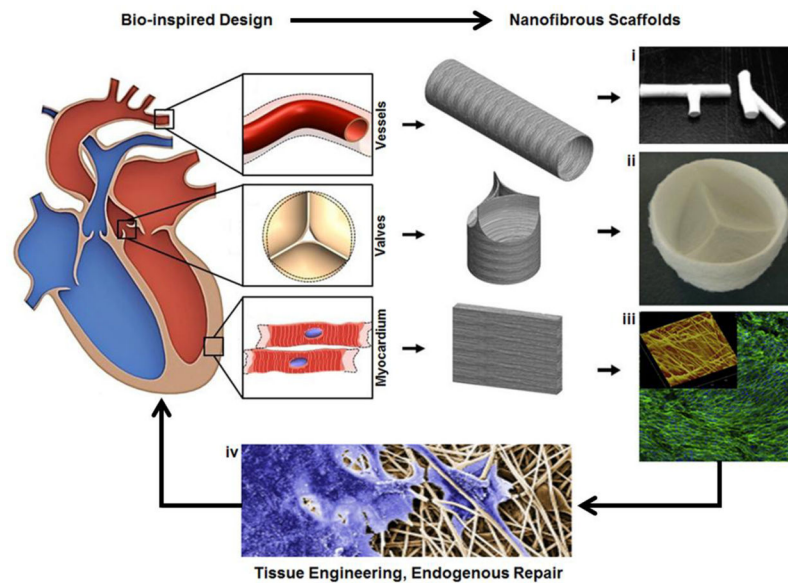
Fig. 6.
Overview of bio-inspired fibrous scaffold fabrication for cardiac tissue engineering. Native cardiac tissue structure and function provide design criteria for engineered fibrous scaffolds. Synthetic vessel, valve, and myocardial scaffolds have each been produced: (i) Electrospun 3D nanofibrous tubes with controllable architectures. Reprinted from [218] with permission from American Chemical Society Publications. (ii) Electrospun trileaflet valve scaffold. Reprinted from [219] with permission from Elsevier; (iii)Confocal micrograph electrospun scaffolds seeded with H9C2 cardiomyoblasts demonstrating cell alignment (Green: F-actin (phalloidin), blue: nuclei (DAPI)), inset shows an atomic force microscopic (AFM) image of the scaffold's 3D surface topography. Scanning area is 50×50 μm. Reprinted from [212] with permission from Elsevier; (iv) Valve interstitial cells infiltrating electrospun scaffolds (SEM colored). Reprinted from [217] with permission from Elsevier.

Table 1

Reference values for the human left ventricle[*]

Measurement	Normal Range
Diastolic diameter	2.4–3.2 cm
Diastolic volume	35–75 mL/m^2
Systolic volume	12–30 mL/m^2
Ejection fraction	67 ± 8 %
Septal wall thickness	0.6–1.0 cm
Posterior wall thickness	0.6–1.0 cm
End-diastolic volume	70 ± 20 mL/m^2
End-systole volume	24 ± 0 mL/m^2
Systolic pressure	90–140 mmHg
Diastolic pressure	6–12 mmHg

[*] Values obtained from Otto et al.[115]

Author Manuscript

Author Manuscript

Table 2

ECM bioprotein composition of rat hearts[*]

ECM Protein	Percent of total ECM Composition		
	Fetal[†]	Neonatal[§]	Adult[¶]
Fibronectin	26	21	4
Laminin	0	5	14
Periostin	7	4	1
Collagen-1	11	16	38
Collagen-3	0	0	4
Collagen-4	8	6	5
Collagen-5	0	6	2
Collagen-6	11	0	6
Emilin-1	4	6	0
Fibrillin-1	13	18	18
Fibrillin-2	8	8	0
Perlecan	12	10	8

[*] Values obtained from Williams et al.[116]: Sprague-Dawley rats,

[†] Fetal: Embryonic day 18–19,

[§] Neonatal: Postnatal day 2–4,

[¶] Adult: ~3 months old

Author Manuscript

Author Manuscript

Table 3

Myocardial conduction velocity

	Conduction Velocity (cm/sec)	Ref.
Human LV	Pacing interval 1000 ms: (CV$_L$ = 92 ±4, CV$_T$ = 22 ±2) Pacing interval 288 ms: (CV$_L$ = 73 ±4, CV$_T$ = 11 ±3) CV$_L$ = 80±8, CV$_T$ = 23±3 (epicardial)	[85] [85] [117]
Pig LV	CV$_L$ = 67 ± 1.9, CV$_T$ = 30 ± 1, CV$_N$ = 17 ± 0.4 CV$_L$ = 50 ± 2, CV$_T$ = 21 ± 1 (epicardial): After 3 to 5 min of global ischemia, CV$_L$ and CV$_T$ decreased to approximately 30 and 13 cm/sec, respectively	[86] [118]
Rat LV	CV$_L$ = 69 ± 13, CV$_T$ = 33 ± 6 CV$_L$ = 34.6+4.5, CV$_T$ = 19.0+4.3,	[119] [120]
NRVM anisotropic tissues	CV$_L$ = 30.5+4.1, CV$_T$ = 13.4+2.7 (Isotropic CV = 21.2+3.7)	[121]
NRVM muscular thin films	Isotropic: CV$_L$ = 15 ± 5, CV$_T$ = 15 ± 4 Anisotropic: CV$_L$ = 20 ± 7, CV$_T$ = 10 ± 2	[10]
mESC-CM	CV = 19.2 ± 0.4	[122]
hESC-CM	CV = 25.1 for 90% CM purity CV = 9.76 ±1.0 for 48–65% CM purity	[123]

Abbreviations: CV$_L$, longitudinal conduction velocity; CV$_T$, transverse conduction velocity; CV$_N$, normal conduction velocity; CM, cardiomyocyte; hESC-CM, human embryonic stem cell derived cardiomyocyte; LV, left ventricle; mESC-CM, mouse embryonic stem cell derived cardiomyocyte; NRVM, neonatal rat ventricular myocyte; SL, sarcomere length.

Table 4

Myocardial contractile stress

	Contractile stress (kPa)	Ref.
Human LV	109.5 (remote from MI), 73.1 (adjacent to MI)	[124]
Rat LV	12.1 ± 0.9 (peak of developed stress, SL = 1.97 ± 0.01 μm) 11.0 ± 0.8 (peak systolic midwall stress)	[125] [126]
Human ventricular muscle strips	Normal, VO: 44 ± 11.7, 19.9 ± 3.7	[127]
Rat left ventricular papillary muscles	56.4 ± 4.4	[127]
NRVM-based muscular thin films	Peak: 15.4 ±1.4, Twitch: 12.7 ± 1.1	[128]
hESC-CM	11.8 ± 4.5 (Force: 5.7 ± 1.0 nN/cell)	[123]
Adult rat CM	41.6 ± 5.6	[129]
AGVM	EPI, SL = 1.9: (T_{pass}, T_{max}) = 0.5 ± 0.1, 25 ±4 EPI, SL = 2.3: (T_{pass}, T_{max}) = 1.5 ± 0.2, 23 ± 3 ENDO, SL = 1.9: (T_{pass}, T_{max}) = 0.6 ± 0.1, 22 ±4 ENDO, SL = 2.3: (T_{pass}, T_{max}) = 2.4 ± 0.2, 20 ± 3	[94]

Abbreviations: AGVM, adult guinea pig ventricular myocytes; CM, cardiomyocyte; ENDO, endocardial; EPI, epicardial; hESC-CM, human embryonic stem cell derived cardiomyocyte; LV, left ventricle; mESC-CM, mouse embryonic stem cell derived cardiomyocyte; MI, myocardial infarction; NRVM, neonatal rat ventricular myocyte; SL, sarcomere length; T_{pass}, passive tension; T_{max}, maximum tension; VO, volume overload

Table 5

Myocardial stiffness

	Stiffness Modulus (kPa)	Ref.
Human LV	ES = 18.3 ± 4.1, ED = 15.0 ± 3.2 (assuming E = 3μ) ED: 24.9 ±2.2	[130] [131]
Pig LV	ES = 28.0 ± 5.7, ED = 18.1 ± 5.6 (assuming E = 3μ)	[103]
Human ventricular muscle strips	PO, VO: 137.2, 51.4 (extension = 0.05) PO, VO: 85.5, 18.8 (extension = 0.2)	[106]
Human ventricular muscle, filament-extracted strips	PO, VO: 28.1, 10.7 (extension = 0.05) PO, VO: 97.8, 43.6 (extension = 0.2)	[106]
Adult human CM obtained from endocardial ventricular biopsies	PO, Normal, VO: 154.6, 59.1, 20.7 (extension = 0.05) PO, Normal, VO: 90.3, 47.8, 46.8 (extension = 0.2)	[106]

Abbreviations: CM, cardiomyocyte; E, elastic modulus; ED, end-diastolic; ES, end-systolic; LV, left ventricle; PO, pressure overload; VO, volume overload; μ, shear modulus.

Table 6

Strain in the human left ventricle (LV)

Strain values	Ref.
Average peak shortening in the LV at endocardium, midwall, epicardium	
44% ±6, 30% ±6, 22%±5	[132]
32% ±4, 23% ±4, 16% ±4	[133]
Peak shortening at the middle ventricular level about the circumference	
15% ± 4 to 19% ± 5	[134]
18% ± 3 to 26% ± 3	[133]
Longitudinal peak shortening about the middle LV circumference at midwall	
12% ± 5 to 13% ±6	[134]
16% ± 3 to 18% ±3	[133]

Table 7

Human valve properties

Parameter	Values	Ref.
Mechanical Properties		
Native Biaxial Aortic Valve Stiffness	CIRCUMFRENTIAL (kPa) Low-Strain (0–18%): 89.1±4.63 Mid-Strain (18–28%): 825.11±29.19 High Strain (28–35%): 1577.17±53.69 RADIAL (kPa) Low-Strain (0–18%): 33.94±1.37 Mid-Strain (18–28%): 116.43±4.15 High Strain (28–35%): 324.93±9.84	[154]
Native Biaxial Pulmonary Valve Stiffness	CIRCUMFRENTIAL (kPa) Low-Strain (0–18%): 11.31±0.79 Mid-Strain (18–28%): 408.23±18.34 High Strain (28–35%): 1457.19±58.1 RADIAL (kPa) Low-Strain (0–18%): 11.67±0.61 Mid-Strain (18–28%): 50.16±2.01 High Strain (28–35%): 172.44±5.24	[154]
Load Durability	40 million loading cycles/year, 3 billion loading cycles/life	[155]
Aortic Valve Flow Rate (systole, healthy)	1.35±.035 m/s (highest flow rate of valves)	[156]
Mitral Valve Flow Rate (diastole, healthy)	0.89±0.15 m/s	[157]
Pulmonary Valve Flow Rate (systole, healthy)	0.6–0.9 m/s	[158]
Tricuspid Valve Flow Rate (diastole, healthy)	0.7 m/s (lowest flow rate of valves)	[159]
Max Closing Strain Rate (diastole, loaded)	Peak Strain Rate: 1000%/s	[160]
Peak Tension Values (general valve tissue range)	Peak Loading Range: 50–100 N/m	[161]
Transvalvular Pressures (back pressures)	Aortic Valve: 80mmHg Pulmonary Valve: 10mmHg Mitral Valve: 120mmHg Tricuspid Valve: 25mmHg	[161]
Valve Area Normal	Aortic Valve: 4.6±1.1cm^2 Mitral Valve: 7.8±1.9cm^2 Pulmonary Valve: 4.7±1.2cm^2 Tricuspid Valve: 10.6±2.6cm^2	[115]
Shear on Aortic Valve (aortic surface, systole)	20 dyn/cm^2	[162]
ECM Properties		
Endothelial Cells (stain and western)	Morphology: Characteristic cobblestone morphology in vitro Immunohistochemistry and Western: 1 vWF- granular and perinuclear 2 Vimentin- uniform distribution 3 DAPI- large and rounded nuclei No Staining: 1 αSMA 2 Myosin and desmin	[163] [161]

Parameter	Values	Ref.
Interstitial Cells (stain and western)	Morphology: Mixture of spindle and rhomboid shaped cells, rapid proliferation in vitro Immunohistochemistry and Western: **1** Vimentin- strong and uniform distribution (fresh & culture) **2** αSMA- strong staining (in culture, not fresh) **3** DAPI- large and rounded nuclei **4** Weaker stains for myosin, calponin, and h-caldesmon (not seen in fresh explants) No Staining: **1** Desmin **2** vWF	
Native Matrix Composition (histology)	**1** Vimentin uniformly expressed throughout the layers of the valve **2** αSMA, myosin, and calponin only found in ventricularis **3** Single cell layer endothelialization (vWF) **4** Collagen primarily in the fibrosa, arranged parallel to the free edge of leaflet (circumferentially aligned); 10–80μm depth; loading during diastole **5** Elastin primarily in the ventricularis, arranged perpendicular to the free edge of the leaflet (radially aligned); 5–30μm depth; elastic recoil during systole **6** Hydrated glycosaminoglycans in spongiosa, lubrication' for the fibrosa and ventricularis layers	

Table 8

Scaffold Fabrication Techniques

Scaffold Fabrication Technique	Design Advantages	Manufacturing Limitations
Decellularized Tissues and Organs	• Purely extracellular matrix • Exact multiscale structure	• Immature cells within a mature matrix • Non-uniform decellularization protocols • Lack of standards for successful decellularization • Variable sample composition • Variable sample quality and sourcing • Requires conductive polymers and solvents
Electrospinning	• Diversity of materials and solvents • Control of fiber morphology (nano to macro) • Nano-micro scale fiber fabrication	• Reliance on high voltage for fiber formation • Low production rates • Reproducible fiber production requires environmental control
Force Spinning (Rotary Jet Spinning)	• Diversity of materials and solvents • Control of fiber morphology (nano to macro) • Nano-micro scale fiber fabrication • Moderate production rate	• Reproducible fiber production requires environmental control

Table 9

Properties of fibrous scaffolds used in cardiac tissue engineering

Manufacturing Method	Composition	Key Scaffold Properties	Application	Ref.
Decellularization	Decellularized porcine myocardium	• Thickness: $2.27 \pm 0.38\mu m$ • Surface Area: $577.45 \pm 44.5mm^2$ • Pore Size: $21.4 \pm 16.8\mu m$ • Proteins Maintained: collagen and elastin • Trapped Water Content: $90.21 \pm 2.36\%$ • Stiffness: 9.5 ± 1.5 MPa in fiber direction and 3.3 ± 0.8 MPa in cross fiber direction	Cardiac tissue engineering	[203]
Decellularization	Decellularized porcine myocardium	• Pore Size: $19.5 \pm 17.9\mu m$ • Thickness: 2mm • Vasculature: $\emptyset 100 - 400\mu m$ • Decell Stiffness: 5.2 ± 1.7MPa • Recell Stiffness: 760.6 ± 69.7kPa	Thick cardiac patch tissue engineering	[204]
Decellularization	Decellularized porcine aortic valve	• Proteins Maintained: fibronectin, vWF, collagen, GAGs present but reduced • Circ. Elastin Stiffness: 763 ± 219 kPa • Circ. Collagen Stiffness: 21 ± 9.3 MPa • Rad. Elastin Stiffness: 352 ± 65 kPa • Rad. Collagen Stiffness: 1.29 ± 0.27 MPa	Aortic valve tissue engineering	[205]
Decellularization	Decellularized collagen *or* Decellularized elastin from porcine aorta	• Pore Size (elastin): 10–	Cardiovascular Tissue Engineering	[206]

Manufacturing Method	Composition	Key Scaffold Properties	Application	Ref.
		40 × 30–120µm • Pore Size (collagen): diameter = 3 – 20 µm • Tensile Strength (elastin): 269 ± 9 kPa • Tensile Strength (collagen): 167 ± 26 kPa • Extensibility (elastin): 1.08 ± 0.02 • Extensibility (collagen): 0.22 ± 0.01		
Decellularization	Decellularized whole rat heart	• Proteins Maintained: collagen I, collagen III, laminin, fibronectin • Decell Stiffness: ~600kPa • Myofiber Size: 250µm – 1.1mm thick	Whole heart tissue engineering	[207]
Decellularization	Decellularized porcine omentum + Au nanoparticles	• Fiber Diameter: 100nm – >1µm • Au nanoparticle Size: 4 or 10nm • Scaffold Stiffness: ~10 – 15MPa	Conductive cardiac patch tissue engineering	[208]
Decellularization	Decellularized human pericardium	• Non X-linked Compressive Strength: 19.7 ± 2.1kPa • X-linked Compressive Strength: 33.7 ± 4.3 kPa • Pore Size: 70 ± 12µm • Porosity (percentage): 98.2%	Cardiac patch tissue engineering (human sourced)	[209]

Manufacturing Method	Composition	Key Scaffold Properties	Application	Ref.
Decellularization	Decellularized whole human heart	• Decell Mass: 85% of donor heart • Structure: vasculature, chordae tendineae, valve leaflets, papillary muscles, and alignment of myocardial fibers maintained • dP/dV Compliance: 84% after decell in LV and 27% in RV	Whole human heart cardiac tissue engineering	[210]
Electrospinning	Poly(lactic-co-glycolic) acid + laminin derived peptides	• Fiber Diameter: ~412 – 1248nm dependent on solution viscosity (4– 8w/v%) • Fiber Alignment: 67.1% fibers aligned within ±30 degrees of axis of alignment • Peptide Density: 3.23 ± 0.068nmol/cm^2 (normalized to fiber surface area)	Cardiac patch tissue engineering	[211]
Electrospinning	Poly(lactic-co-glycolic) acid *or* Polycarbonate -urethane	• Fiber Diameter (PLGA): 280.4 ± 96.5nm • Fiber Diameter (PCU): 699.4 ± 201.1nm • Stiffness (PLGA): 50 – 300 MPa dependent on target collected on • Stiffness (PCU): 0.5 – 2.0 MPa dependent on target collected on	Regenerative cardiac tissue engineering	[212]
Electrospinning	Poly(ε-caprolactone)	• Stiffness (straight fiber): ~0.15MPa	Cardiac patch tissue engineering	[213]

Manufacturing Method	Composition	Key Scaffold Properties	Application	Ref.
		• Stiffness (spring fiber): ~0.05MPa • Extensibility (straight fiber): ~115% • Extensibility (spring fiber): ~275% • Pore Area (straight fibers): 1000μm^2 • Pore Area (spring fibers): 4000μm^2, diameter ~70μm		
Electrospinning	Poly(glycerol sebacate) – poly(ε-caprolactone) + VEGF	• Fiber diameter: 0.8 ± 0.3μm • Pore Size: 2.2 ± 1.2μm • Porosity (percentage non-scaffold): 62 ± 4% • Hydraulic Permeability: 4×10^{-6}cm/(sPa) • Intrinsic Permeability: 2×10^{-3} Darcy • Stiffness: 8 ± 2MPa • Ultimate Tensile Strength: 3 ± 0.5MPa at 142 ± 29% strain • Protein concentration: 1.0μg/cm^2	Cardiac patch tissue engineering	[214]
Electrospinning	Poly(glycerol sebacate) – poly(ε-caprolactone)	• Fiber Diameter: ~3.5 – 10μm dependent on polymer ratios • Pore Size: ~40–5010μm dependent on polymer ratios • Stiffness (parallel to fiber axis): 4.16 ± 1.0 – 9.28 ± 0.43MPa dependent on polymer ratios	Cardiac valve tissue engineering	[215]

Manufacturing Method	Composition	Key Scaffold Properties	Application	Ref.
		• Stiffness (perpendicular to fiber axis): $0.95 \pm 0.68 - 1.21 \pm 0.33$MPa dependent on polymer ratios		
Electrospinning	Poly(ester urethane)urea	• Fiber Alignment: >0.6 orientation index • Ultimate Tensile Strength (circ): $12.2 - 16.2$MPa dependent on collection technique • Ultimate Tensile Strength (rad): $3.3\pm1.3 - 6.4\pm1.1$MPa dependent on collection technique • Suture Retention Strength: $64.9\pm6.2 - 102\pm8.4$ N/mm^2 dependent on collection technique	Pulmonary valve tissue engineering	[216]
Electrospinning	Poly(ethylene glycol) dimethacrylate - poly(l-lactide)	• Fiber Diameter: 0.37 ± 0.08μm • Stiffness: 141 ± 23.6MPa • Ultimate Tensile Strength: 2.1 ± 0.3MPa • Extensibility: 4 ± 0.4% • Pore Size: 8.24 ± 6.23μm^2 • Swelling Ratio: 59 ± 6% • Contact Angle (water): 38.7 ± 10.9°	Cardiac valve tissue engineering	[217]
Force Spinning (RJS)	Poly(lactic acid) *or* Gelatin	• Fiber Diameter (PLA): $424 \pm 41 - 1143 \pm 50$nm dependent on	Cardiac tissue engineering	[28]

Manufacturing Method	Composition	Key Scaffold Properties	Application	Ref.
		• fiber extrusion speed • Fiber Diameter (gelatin): 515 ± 27nm		
Force Spinning (RJS)	poly(ε-caprolactone) - Gelatin	• Fiber Diameter: ~0.4 – 1.5μm dependent on polyer:protein ratio (increasing with increasing protein content) • Fiber Alignment: ~0.9 – 0.5 orientation order parameter, dependent on polyer:protein ratio (decreasing with increasing protein content) • Stiffness (75/25 PCL/ Gelatin): ~15MPa • Stiffness (PCL): ~300MPa	Cardiac Tissue Engineering	[29]

Table 10

Effects of fibrous scaffolds used for cardiac tissue engineering

Scaffold material	Key scaffold properties	Cell sources	Key experimental results	Ref.
Electrospun PLLA and PLGA	PLGA membranes were uniaxially stretched to achieve anisotropic fiber architectures	NRCM isolated from 2–4 day old Sprague-Dawley rats	In vitro: Cardiomyocyte isotropic or anisotropic growth controlled by fiber structural cues	[234]
Electrospun polyester blend (PHBV (5% HV), P(L-D,L)LA (70:30) and PGS)	Included biodegradable macroporous tubes to perfuse the scaffold	hMSC from human umbilical cord	In vitro: Fibers aligned MSCs, perfusion of medium through macroporous tubes increased MSC viability	[235]
Electrospun PCL/gelatin	Biodegradable nanofibrous cardiac patch. Nanofiber diameter = 244 ± 51 nm	MSC isolated from rat bone marrow	Rat Model: Patch reduced scar size and increased vessel density in MI model.	[236]
Electrospun PCL	Plasma surface functionalized	MSC	Rat Model: Patch attenuated dilatation in MI model. Ejection fraction decrease was 6% in patched hearts vs 13% in sham	[237]
Electrospun PLGA and thermoplastic polycarbonate-urethane (PCU, Bionate®)	Textile-templated	H9C2 rat cardiac myoblast cell line, NRCM isolated from 1–3 day old Sprague-Dawley rats	In vitro: Myocyte alignment, elongation, and improved contractile synchrony on templated scaffolds	[212]
Electrospun PGS/gelatin with embedded carbon nanotubes (CNT)	CNT: 0 to 1.5%	NRCM isolated from 2 day old Sprague-Dawley rats	In vitro: CNT inclusion reduced excitation threshold and increased maximum capture rate	[226]
Assembly of alginate + gold nanowires (NW) composite	Macroporous hydrogel, Compressive moduli (kPa): Alg: 1.2±0.2 Alg+NW: 3.5±0.2	NRCM (0–1 day old)	In vitro: Gold NW inclusion improved engineered cardiac tissue contractile synchronicity	[225]
PLGA hydrogel cast on force-spun fibrous sucrose templates	PLGA solutions were cast on extrusion-spun fibrous sucrose templates. Sucrose was subsequently leached.	NRCM isolated from 2–3 day old Sprague-Dawley rats	In vitro: Anisotropic cell alignment and electrical propagation. Two-fold higher conduction velocity along vs. across cardiac fibers	[233]
PGS hydrogel synthesized by polycondensation of glycerol and sebacic acid	PGS materials synthesized at 110, 120 and 130 °C had Young's moduli of 0.056, 0.22 and 1.2 MPa, respectively	Acellular	In vitro: Demonstrated a range of controllable stiffness and degradation kinetics	[238]
Commercial porous collagen sponge hydrogel	Cytokine-conjugated system: Covalently-immobilized proangiogenic cytokines (VEGF, bFGF)	hMSC from young (50.0 ± 8.0 years, N = 4) or old (74.5 ± 7.4 years, N = 4) donors	In vitro: Enhanced cell proliferation Rat Model: Prolonged cell survival and improved angiogenesis following surgical ventricular restoration. Ejection fraction correlated with cell survival, patch thickness, and vascular density	[239]
Compressed type I collagen hydrogel	Hydrogels were compressed to achieve compressive modulus, E_c~5 kPa	Acellular	Rat Model: Attenuated left ventricular remodeling, diminished fibrosis, and enhanced blood vessel formation following myocardial infarct	[224]

Abbreviations: bFGF, basic fibroblast growth factor; CNT, carbon nanotubes; GAG, glycosoaminoglycan; MI, Myocardial infarction; MSC, mesenchymal stem cell; hMSC, human mesenchymal stem cell; NRCM, neonatal rat cardiomyocyte; PCL, polycaprolactone; PGA, poly(glycolic acid);PGS, poly(glycerol sebacate); PHBV, Poly(3-hydroxybutyrate-co-3-hydroxyvalerate); PLGA, poly(lactic-co-glycolic) acid; PLLA, poly(L-lactic acid); POC, poly(1,8-octanediol-co-citric acid); VEGF, vascular endothelial growth factor